Journal Pre-proofs

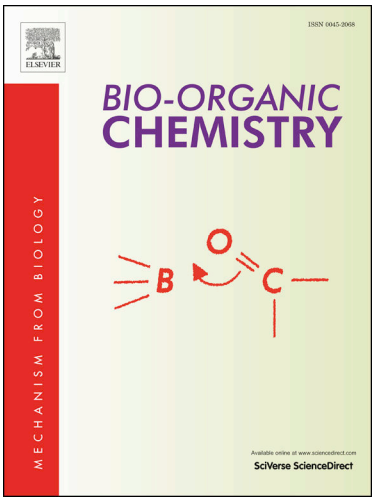

Synthesis, ^{18}F-Radiolabeling and Apoptosis Inducing Studies of Novel 4, 7-Disubstituted Coumarins

Nerella Sridhar Goud, Venkata Krishna Kanth, Jakkula Pranay, Ravi Alvala, Insaf A. Qureshi, Pardeep Kumar, Rose Dawn Bharath, Chandana Nagaraj, Suresh Yerramasetti, Manika Pal-Bhadra, Mallika Alvala

PII: S0045-2068(20)30035-3
DOI: https://doi.org/10.1016/j.bioorg.2020.103663
Reference: YBIOO 103663

To appear in: *Bioorganic Chemistry*

Received Date: 6 January 2020
Revised Date: 23 January 2020
Accepted Date: 11 February 2020

Please cite this article as: N. Sridhar Goud, V. Krishna Kanth, J. Pranay, R. Alvala, I.A. Qureshi, P. Kumar, R. Dawn Bharath, C. Nagaraj, S. Yerramasetti, M. Pal-Bhadra, M. Alvala, Synthesis, ^{18}F-Radiolabeling and Apoptosis Inducing Studies of Novel 4, 7-Disubstituted Coumarins, *Bioorganic Chemistry* (2020), doi: https://doi.org/10.1016/j.bioorg.2020.103663

Synthesis, ^{18}F-Radiolabeling and Apoptosis Inducing Studies of Novel 4, 7-Disubstituted Coumarins

Nerella Sridhar Goud [a, b], Venkata Krishna Kanth [c], Jakkula Pranay [e], Ravi Alvala [d], Insaf A. Qureshi [e], Pardeep Kumar [b], Rose Dawn Bharath [b], Chandana Nagaraj [b], Suresh Yerramasetti [c], Manika Pal-Bhadra [c], Mallika Alvala [a]*

[a] Department of Medicinal Chemistry, National Institute of Pharmaceutical Education and Research (NIPER), Hyderabad 500 037, India.

[b] Department of Neuroimaging and Interventional Radiology (NI & IR), National Institute of Mental Health and Neuro Sciences (NIMHANS), Bangalore 560 029, India.

[c] Department of Applied Biology, CSIR-Indian Institute of Chemical Technology, Hyderabad 500 007, India.

[d] G. Pulla Reddy College of Pharmacy, Hyderabad 500 028, India.

[e] Department of Biotechnology & Bioinformatics, School of Life Sciences, University of Hyderabad, Hyderabad 500 046, India.

*Corresponding Address:

Dr. Mallika Alvala (PhD)
Faculty of Medicinal Chemistry
NIPER-Hyderabad
Email: mallikaalvala@yahoo.in

Abstract:

In present study, a new series of 4, 7-disubstituted coumarin derivatives **(7a-y)** have been synthesized as galectin-1 targeting apoptosis inducing agents and evaluated for their *in vitro* cytotoxic potentials against a panel of selected human cancer cell lines namely, Brest (MCF7), Ovarian (SKOV3), Prostate (PC-3 & DU145) and normal embryonic kidney (HEK293T) cells, using MTT assay. Most of the compounds exhibited potent growth inhibitory action against the treated cancer cell lines with an IC_{50} range of 10-30 μM. Compound **7q** exhibited a significant growth inhibition against prostate cancer (PC-3 & DU145) cell lines with an IC_{50} value of 7.45±0.03 μM, 8.95±0.17 μM respectively. Further, the target compound **7q** was radiolabeled with fluorine-18 [^{18}F] to be used as a novel PET radiotracer for imaging of tumors *via* targeting galectin-1, using appropriate reaction conditions in the GE Tracer-lab FX2N synthesis module. The purification of the [^{18}F] radiolabeled compound **[^{18}F]-7q** was successfully achieved with 60% ethanol. The radiochemical purity was greater than 85 % and residual solvent limits of DMF was 65 ± 3 ppm as analysed by HPLC, TLC & GC analytical methods. The apoptosis studies confirm the inhibition of cell proliferation with morphological changes like cell shrinkage, blebbing and cell wall deformation, increasing the ROS levels, and loss of mitochondrial membrane potential by Acridine orange/Ethidium bromide staining, Hoechst-33342 staining**,** H_2DCFDA staining, annexin V-FITC/PI, and JC-1 staining methods. In flow cytometric analysis, **7q** selectively arrested the sub-G1 phase of the cell cycle in a dose-dependent manner. In Gal-1 ELISA studies, compound **7q** efficiently reduced the levels of Gal-1 protein in dose-dependent manner with an IC_{50} value of 100 μM. The binding constant (K_a) of **7q** with Gal-1 was observed as 1.3 x 10^4 M^{-1} by fluorescence spectroscopy. The molecular docking studies clearly showed possible interactions and the pharmacokinetic (ADMET) properties of compound **7q** with Gal-1. Hence, the novel 4, 7-disubstituted coumarins could be a potential cytotoxic and PET imaging agents *via* Gal-1.

Key Words: 4-substituted coumarins, fluorine-18, positron emission tomography, galectin-1, cancer, apoptosis.

Research Highlights:

- The **7q** is a novel anticancer agent with an IC_{50} of 7.45±0.03 μM mediated by Gal-1 in PC-3 cells.

- Identified novel **7q** molecule which induces apoptosis *via* Gal-1 reduction in PC-3 cells.
- The **[^{18}F]-7q** radiotracer is an ideal PET imaging agent due to its optimal half-life of 110 min.
- The radiochemical identity and purity were confirmed as per cGMP guidelines for clinical use.

1. Introduction

Cancer is one of the life-threatening diseases in the world and characterized by uncontrolled cell division. According to the World Health Organization (WHO), it is estimated to have a rise of over 13 million by 2030 [1, 2]. Drug-induced toxicity, poor selectivity, and tolerance of the current chemotherapeutic agents necessitate the development of new anticancer agents with different mechanisms. The critical cellular process which plays an important role in tissue growth maintenance and homeostasis is apoptosis [3]. Many studies have suggested that the tumor cell death induction through apoptosis reserves a physiological advantage in cancer therapy [4]. Human Galectin-1 (Gal-1) gained interest due to its key role in biological events like angiogenesis, metastasis, apoptosis, and invasion of tumor cell [5]. Gal-1 is a protein of galectin family binds to cell-surface and extracellular matrix glycan and affects cellular functions [6]. The interaction of gal-1 with glycans plays a major role in cancer biology and tumor immunity. Gal-1 is lower expressed in normal cells and blood, but it is overexpressed in neoplastic diseases [7]. The Gal-1 has been reported to overexpress in many cancer types *viz.* prostate, breast, lung, melanoma and renal, *etc.* [8, 9]. Gal-1 is considered as a biomarker in diagnosis, prognosis and treatment condition of various cancer & neurological conditions. Hence, the Gal-1 is regarded as a molecular target to develop newer therapeutic agents with increased safety and efficacy for cancer therapy.

The diagnosis with target based positron emission tomography (PET) imaging agent is a powerful tool for early detection and diagnosis of the condition to the next treatment level. Therefore, it is necessary to focus on radiochemical synthesis and quality control studies based on the importance of PET imaging modality for diagnosis [10]. The 18F labeled radiotracers are emerging as potential weapons for the diagnosis, prognosis and therapy monitoring of various neurological and tumor-associated conditions through PET imaging quantitative modality [11]. 18F isotope is highly feasible in the radiolabelling of bioactive molecules for PET imaging since it has positron-emitting property and favourable half-life of

110 min unlike other isotopes [12]. The USFDA approved a biologically active molecule with 18F (Fluorodeoxyglucose-FDG) has gained more significance in the diagnosis and progression of various tumor cells & neurological conditions using PET [13]. The 18F radiotracers provide PET images of cellular uptake, transport, neurotransmission and, metabolic processes on the molecular level in the body. which also act as powerful weapons to identify new drug targets through pharmacodynamics and pharmacokinetic (ADME) properties of drugs *in-vivo* [14, 15]. *Ewelina Kluza et al*, have reported that the synergistic targeting of both $\alpha_v\beta_3$ and galectin-1 improves the specificity of fluorescent liposomes to tumor endothelium *in vivo*, which can be easily accessed to Magnetic Resonance Imaging (MRI) modality for high-resolution tumor images [16].

Coumarin (2H-chromen-2-one), neoflavonoid group of plant secondary metabolites, and consists of fused benzene with 2-pyrone ring. A wide variety of natural and synthetic coumarin derivatives with diverse pharmacological activities *viz.* anticoagulant, antibacterial, antioxidant, anti-HIV, antitubercular, antihyperglycemic, anticonvulsant, anti-hypertensive, anti-inflammatory, and anticancer have been reported [17, 18]. Coumarin derivatives are widely explored for anticancer activities as they possess limited side effects and multidrug reversal activity. It is proved that the substitution at C-3, C-4 & C-7 positions of coumarin exhibits tremendous anticancer activities, whereas at C-5, C-6 & C-8 positions showed less anticancer potentials against a wide range of cancer cell lines [19]. Coumarin derivatives with C-4 substitution target essential pathways to treat cancer such as HSP90 inhibition, 17βHSD3 inhibition, protein kinase inhibition, aromatase inhibition, TNF-α inhibition, cell cycle arrest, apoptosis induction, DNA intercalation and microtubulin inhibition [20]. Recently, our research group has reported a new series of heterocyclic imines linked coumarin-thiazole hybrids as anticancer agents (**1**) by targeting Gal-1 with an IC_{50} of 300 μM [21]. *Dong Cao et al,* have reported 4-substituted coumarin derivatives (**II**), as potential anticancer agents with an IC_{50} value ranges from 7-47 nM [22]. *Rajput et al.,* have reported coumarin based glycoside derivatives as galectin inhibitors. The coumarylmethyl galactoside (**II**) derivative showed greater affinity towards various selected galectins [23]. *Huiping Zhao et al,* have reported optimization of the novobiocin Scaffold to produce anti-proliferative agents and developed a new series of novobiocin analogues (**IV**) as selective Hsp90 inhibitors through various structural modifications in the sugar moiety by sugar mimics, and piperidine, an aza sugar mimics incur anticancer activity in nM range against a panel of cancer cell lines (**Fig. 1**) [24].

<insert Figure 1 here>

The diagnosis with target based PET radiotracer is a powerful tool for early detection, and understand the disease condition. Hence, overexpression of Gal-1 at different stages in multiple cancer cells & importance of PET imaging modality for diagnosis, have triggered our interest to develop novel 4, 7-disubstituted coumarin derivatives. Therefore, the present study aims in synthesis, ^{18}F-radiolabeling of novel 4, 7-disubstituted coumarins and *in-vitro* biological evaluation against a panel of cancer cells with selective galectin-1 inhibition.

2.0. Results and Discussion

2.1. Chemistry

The target coumarin analogues **(7a-y)** were synthesized by refluxing various aromatic and aliphatic halides with different cyclic saturated rings conjugated coumarins **(4a, 4b, 5a, 5b, 6a)** as showed in **Scheme 1**. Initially, the 4-(chloromethyl)-7-hydroxy-2H-chromen-2-one **(3)** was synthesized by pechmenn condensation of resorcinol **(1)** and ethyl-4-chloroacetoacetate **(2)** in the presence of sulphuric acid [25]. In the next step, the 7-hydroxy-4-(substituted morpholinomethyl)-2H-chromen-2-ones **(4a, 4b)**, 7-hydroxy-4-(substituted piperidinomethyl)-2H-chromen-2-ones **(5a, 5b)** and 4-((3,4-dihydroisoquinolin-2(1H)-yl) methyl)-7-hydroxy-2H-chromen-2-one **(6a)** were synthesized by N-alkylation [26] of substituted morpholines, piperidines and tetrahydroisoquinoline with compound **(3)**. Finally, the O-alkylation of compounds **(4a, 4b, 5a, 5b, 6a)** with various aromatic and aliphatic halides, in the presence of potassium carbonate furnishing the target compounds **7a-y** with moderate to good yields.

<Insert scheme 1 here>

All synthesized compounds (**7a-y**) were characterized by analytical techniques *viz.* HRMS, ^{1}H and ^{13}C NMR Spectroscopy. The ^{1}H NMR spectrum of **7a** showed characteristic protons of O- and N-attached methylene groups of morpholine at δ 2.59 and at δ 3.76. The methylene group protons on the C-4 position of coumarin appeared at δ 3.64 and remaining all protons appeared in the range of δ 5.25-8.50. In the ^{13}C-NMR spectrum of **7a,** the carbonyl and methylene carbon on the C-4 position of coumarin appeared at δ 161.15 and δ 30.97. The remaining carbons appeared in the range of δ 53.80-160.54. A similar fashion was observed in the rest of all other compounds ^{1}H NMR and ^{13}C NMR spectrum **(7a-y).** In addition, the

compounds **7f-j** showed characteristic singlet for dimethyl protons of dimethylmorpholine at δ 1.16 and the compounds **7k-o**, exhibited a sharp singlet of methyl protons of methyl piperidine at δ 1.42. The ester group of piperidine ester derivatives **7p-t** showed a triplet at δ 1.26 and quartet at δ 4.14. The HRMS (ESI) of **7a-y** showed corresponding $[M+H]^+$ peaks based on their molecular weights.

2.2. Radiochemistry

The [^{18}F] fluoride is produced *via* [^{18}O (p, n)^{18}F] nuclear reaction in the cyclotron. Around 350 ± 30 mCi of [^{18}F] radionuclide was transferred from cyclotron to the GE tracer lab FX2N synthesis module and further, it was trapped in Quaternary Ammonium Anion exchange (QMA) cartridge and eluted by kryptofix (K222) solution from QMA and eluted into the reactor (**Fig. 2**). The [^{18}F]-cryptand complex was dried and radiolabeling of **[^{18}F]-7q** was done by aromatic nucleophilic substitution reaction (S_NAr) [27], by reacting the precursor molecule (**7q**) with [^{18}F]-cryptand (K2.2.2) complex in DMF (**Scheme-2**). The yield of the **[^{18}F]-7q** was 5 ± 2% after purification through tC18 cartridge. In the purification process, initially the reaction mixture was washed out with water and 20% ethanol, and the maximum elution was achieved with 60% ethanol. The radiochemical purity was evaluated by High Pressure Liquid Chromatography (HPLC) analysis [28], and, the usual retention time for free [^{18}F] radionuclide is at 4.3 ± 0.7 min and found the retention time of **[^{18}F]-7q** compound at 16.80 ± 0.2 min (**Fig. 3A**). The HPLC retention time for cold target compounds was found at 16.88 ± 0.2 min (**Fig. 3B**). The matching of retention time of cold target compound with **[^{18}F]-7q** compound confirmed the radiolabeling of the precursor molecule (**7q**) and proves that the target compound is our radiolabeled molecule of interest.

<Insert scheme 2 here>

<insert Figure 2 here>

The retention factor was 0.6 for **[^{18}F]-7q** compound on the TLC study. The radiochemical purity for the **[^{18}F]-7q** was around > 85 % as measured by HPLC. The pH of the preparation was 5.5 ± 0.5 as evaluated by pH paper. The levels of the solvent Dimethylformamide (DMF) was evaluated in the final preparation using Gas Chromatography (GC) analysis [29]. The GC analysis showed DMF level was 65 ± 3 ppm (**Fig. 4**). As per the Food Drug Administration (FDA) Q3C(R6) guidelines, the DMF is considered as a class 2-solvent and the acceptable limit is 880 ppm. The levels of the DMF in the final product were in the acceptable limit. The

ethanol content is high as it is an eluting solution. The United States Food and Drug Administration (USFDA) and European Medicines Agency have found the higher amounts of ethanol (> 0.5%, the limit for class 3 residual solvents) in radiopharmaceuticals may be acceptable provided they are synthesized and manufactured under good manufacturing practice [30]. Our study has shown the successful radiolabeling of the **7q** compound with [^{18}F] radionuclide which can target the Gal-1 protein on the overexpressed cells. The novel 4, 7-disubstituted coumarins could be a potential cytotoxic, but the quantity of molecule used for PET imaging is in lower nanogram concentration. The final quantity in the radiolabeled formulation is in nanomoles, therefore, impact of any side effects is very rare. Target based PET diagnosis is the primary choice to know the disease progression and prescribe better medication to the patient, hence we have explored the feasibility of radiolabeling of **7q** with 18F radionuclide, and succeeded in achieving good results. There are many drugs like paclitaxel, gefitinib, erlotinib, doxorubicin has been labeled with ^{18}F, and used as PET imaging agents. These drugs have their own potential side effects but still using as PET tracers in nanomoles [31-34].

<insert Figure 3A & 3B here>

<insert Figure 4 here>

2.3 Biological evaluation:

2.3.1 Cell proliferation and cytotoxicity analysis:

To evaluate the cell proliferative and cytotoxicity of the novel coumarin analogues (**7a-y**), Sulforhodamine B (SRB) cell proliferation assay against a panel of human cancer cell lines namely, Brest (MCF7), Ovarian (SKOV3), Prostate (PC-3 & DU145) and normal embryonic kidney (HEK293T) cells, was performed. Briefly, cells were seeded in 96 well plates with a density of $1*10^4$ cells/well and incubated with target compounds (**7a-y**) for a period of 72 h and fixed with 10% Trichloroacetic acid [35]. Plates were stained with a 0.057% SRB stain solution and eluted with 10mM Tris having pH 10.5. The elute was measured at 510nm with a spectrophotometer. Inhibitory concentrations of the compounds (**7a-y**) were calculated with the sigmoidal curve method and analyzed **(Table 1)**. Overall **7q** showed a prominent inhibition of growth at 7.45±0.03 μM concentration in prostate cancer cell line PC-3. All the experiments were performed in triplicates and Doxorubicin was employed as a positive control. In Structural activity relationship **(SAR)**, the morpholine linked coumarin derivatives **(7a-e)** exhibited moderate cytotoxicity, whereas the dimethyl morpholine linked coumarin

derivatives **(7f-j)** and methyl piperidine linked coumarin derivatives **(7k-0)** showed good cytotoxicity. The piperidine ester linked coumarin derivatives **(7p-t)** exhibited a significant cytotoxicity and isoquinoline linked coumarin derivatives **(7u-y)** exhibited less cytotoxicity. Hence, we have concluded that piperidine ester derivatives (**7p-t**) are promising cytotoxic agents.

<Insert Table 1 here>

2.3.2 Effect of compound 7q on Gal-1 protein levels:

Targeting Gal-1 is considered as one of the emerging approaches for the treatment of cancer, as it plays a vital role in tumor development and metastasis. It is evident from the literature that Gal-1 expression is associated with numerous tumor types [36]. Compound **7q** was examined for its effect on Gal-1 levels. PC-3 cells were grown in 60mm cell culture dishes, treated with **7q** for 48 h and the supernatant was collected. As Gal-1 is *an* extracellular secreted protein, its expression can be quantified from the cellular external environment [37]. Equal amounts of supernatant were subjected to quantitative enzyme immunoassay as per manufacture's protocol [DGAL10, R&D Systems, USA]. In details, the supernatant was incubated with human Gal-1 coated plates and washed to remove unbound protein. Furthermore, an enzyme-linked antibody was added to the reaction, specific to human Gal-1 and incubated with substrate solution for 30minutes before terminating the reaction with 50µl of the stop solution. The amount of protein expression was detected at 450 nm using UV-spectrophotometer. Compound **7q** effectively reduced the levels of Gal-1 in dose-dependent manner at the concentrations of 10, 30, 100 and 300 µM (**Fig. 5**, **Table 2)** and the IC_{50} value found to be 100µM stipulating that the molecular target of these coumarin analogues to be Gal-1.

<Insert Figure 5 here>

<Insert Table 2 here>

2.3.3. Fluorescence studies:

In fluorescence studies, there a decrease in fluorescence intensity with increasing concentration of the compound, and maximum emission spectra of Gal-1 was at 343 nm **(Fig. 6A).** The plot of log[7q] versus $\log(F_o\text{-}F)/F$ had given a linear relationship **(Fig. 6B)** and the number of binding sites was calculated from the slope, which was found to be 0.89 and infers interaction of protein and compound in 1:1 ratio. The binding constant (K_a) was calculated from the intercept value which was observed as 1.3×10^4 M^{-1}. The intensity of the

fluorescence was quenched upon the increase of ligand concentration and the bimolar quenching constant (K_q) was calculated to be 3.8 x 10^{12} M^{-1} s^{-1} which is larger than diffusion control limit [38] suggesting interaction of protein and ligand as well as the mode of quenching to be static.

<Insert Figure 6A & 6B here>

2.3.4 Effect on the Cell cycle distribution:

The **7q** that demonstrated the strong cytotoxic effect on PC-3 cells was further studied for cell cycle analysis using intercalating fluorescent dye, Propidium Iodide (PI) which can be visualized with the aid of fluorescent flow cytometry. PC-3 cells were seeded in 60mm dishes at a density of 5x10^5 cells/plate and treated with **7q at** 5, 7.5, 10µM concentrations for 48 h followed by overnight fixation with 70% ethanol. Cells were further stained with PI and analyzed with the aid of BD Accuri™ C6 flow cytometry for the distribution of cell cycle phases **(Fig. 7A)**. Cells demonstrated an increase in the percentage of the sub-G1 phase of cell cycle upon treatment with **7q** in a concentration-dependent manner with 13.36% at 10µM **(Fig. 7B**). Fluorescent based cell cycle analysis clearly demonstrated an arrest at the sub-G1 phase of cell cycle post-treatment in PC-3 cells.

<Insert Figure 7A & 7B here>

2.3.5 Annexin-V/Propidium iodide dual staining assay:

To establish the extent of cells undergoing apoptosis, Annexin-V/Propidium Iodide staining was employed. Annexin-V is a marker of early apoptotic cells that binds specifically to the protein of phosphatidylserine PS [39]. Cells were grown in 60mm dishes and treated with **7q** for 48h. Thereafter, the cells were trypsinized, stained with Annexin-V/Propidium iodide and analyzed with fluorescent based flow cytometry. Annexin-V/propidium iodide staining reveals the distribution of cells between live, necrotic, early and late apoptotic phases. Cells treated with **7q** for 48 h demonstrated an increased cell population in the apoptotic phase in a concentration dependent manner **(Fig. 8**). At 10µM concentration, approximately 28% of the cells underwent apoptosis.

<Insert Figure 8 here>

2.3.6 Acridine orange/ethidium bromide (AO/EB) staining:

Acridine orange (AO) is a DNA intercalating dye that binds to both live and dead cells, whereas Ethidium bromide (EB) stains only nonviable cells, i.e., cells which have lost the cell

membrane integrity [40]. The green vs red fluorescence clearly demonstrates the extent of cells undergoing apoptosis. Cells were grown on coverslips for 48 h post-treatment with **7q**, stained with AO/EB dual stain and imaged with a fluorescent inverted microscope at 10X magnification. PC-3 cells treated with **7q** initiated apoptosis at 5 µM concentration treatment, with a gradual increase in a concentration-dependent manner i.e., cells at 10 µM showed a clear induction of apoptosis **(Fig. 9**).

<Insert Figure 9 here>

2.3.7 Hoechst-33342 nuclear morphology staining:

Cells undergoing apoptosis or necrosis, develop a condensed or fragmented DNA indicating an ideal mark to distinguish viable and non-viable cells [41]. Hoechst 33342 is a cell-permeable fluorescent benzimidazole dye that stains DNA by binding to the minor groove. To observe morphological changes and to confirm above-mentioned results cells were grown in coverslips and Hoechst staining was performed post-treatment with **7q** for 48 h. Results revealed a clear condensation of DNA as marked by arrows in **Fig. 10**. This clearly demonstrates altered nuclear architecture due to the treatment with 7q in PC-3 cells.

<Insert Figure 10 here>

2.3.8 Effect on the Mitochondrial membrane potential:

The loss of mitochondrial membrane potential distinctly indicates cell apoptosis [42]. As induction of apoptosis by the treatment of **7q** was evidently established we wanted to see the effect on mitochondrial membrane potential. The dysfunction of mitochondria has been long associated with early induction apoptosis and measurement of the depolarization of mitochondria reveals the extent of the induction. JC-1, a carbocyanine cationic dye that accumulates in the mitochondria in a potential-dependent manner i.e., JC-1 forms J-aggregates (red fluorescence) in energized mitochondria whereas loss of membrane potential leads to the formation of JC-1 monomers (green fluorescence) [43]. JC-1 forms J-aggregates in turn emitting red fluorescence in untreated control PC-3 cells, whereas depolarized mitochondria due to the 7q treatment for 48 h emit green fluorescence i.e., the formation of J-monomers **(Fig. 11A)**. Analysis with fluorescent-based flow cytometry revealed that there was increased depolarization of mitochondrial membrane potential upon **7q** treatment **(fig. 11B)**. This data establishes the role of **7q** in the induction of apoptosis through the loss of mitochondrial membrane potential.

<Insert Figure 11A & 11B here>

2.3.9 Estimation of ROS levels by DCFDA fluorescence assay:

Reactive oxygen species (ROS) play a seemingly vital role in physiological as well as pathological conditions including apoptosis [44]. As **7q** has the ability to induce apoptosis, levels of ROS were studied. To evaluate the levels of ROS, the reduced fluorescein, H_2DCFDA (2',7'-dichlorodihydrofluorescein diacetate) was utilized. H_2DCFDA is a non-fluorescent dye, which emits fluorescence upon the breakage of the acetate moieties due to the presence of intracellular esterases. Treatment of the PC-3 cells with **7q** showed a clear elevation in ROS levels as visualized by the emission of green fluorescence by the H2DCFDA dye (**Fig. 12**).

<Insert Figure 12 here>

2.4 Molecular docking Studies:

The interactions of Gal-1 with the compound **7q** were studied by molecular docking calculations using the Glide docking module of Schrodinger suite [45]. The 3D crystal co-ordinates of human Gal-1 were retrieved from the protein data bank (PDB ID: 4Y24). The 2D, 3D ligand interaction, and electronic surface interaction diagrams of **7q** was shown in **Figure 13A, 13B & 13C**. Hydrogen bonding interaction was found at a distance of 3.06Å between NH of Glu71 acting as a donor (atom no. 1518) and C=O of ester moiety of ethyl isonipecotate moiety acting as an acceptor (atom no. 2031). Another hydrogen bond was found at a distance of 2.07Å between OH of Ser29 as a donor (atom no. 1229) and the oxygen of nitro on phenyl acting as an acceptor (atom no. 2040). Further, π- π stacking between the indole ring of Trp68 and coumarin ring and the π-cation stacking interaction between the nitrogen of Arg48(atom no. 354) and the coumarin ring seems to stabilize the docking pose of the **7q** molecule. A set of pharmacokinetic Absorption, Distribution, Metabolism, Elimination (ADMET) related properties were calculated using qikprop program [46]. The physicochemical properties of **7q** matched with the prescribed ranges as represented in **Table 3.** Additionally, the molecular weight (mol. Wt.), hydrogen bond donors (donor HB), hydrogen bond acceptors (accept HB), partition coefficient (QPlogPo/w), exhibited acceptable values that followed Lipinski rule of five.

<Insert Figure 13A, 13B & 13C here>

<Insert Table 3 here>

3.0 Conclusion:

A series of novel 4, 7-disubstituted coumarin derivatives were synthesized **(7a-y)** and cytotoxic activity was evaluated against a panel of cell lines. Amongst all the synthesized conjugates, **7q** exhibited potential anti-proliferative against prostate cancer cell line, PC-3 at a concentration of 7.45±0.03 μM. Cell cycle distribution analysis revealed an arrest at the sub-G1 phase, following treatment with conjugate **7q**. Annexin-V staining revealed an increasing population of cells undergoing apoptosis in a concentration-dependent manner by treatment with conjugate **7q** in PC-3 cells. This was supported by both, Acridine Orange/Ethidium Bromide and Hoechst 33342 nuclear staining. Loss of mitochondrial membrane potential and increased reactive oxygen species, as established by the JC-1 and H_2DCFDA staining, respectively suggest a possible mechanism of action of the conjugate **7q** in inducing apoptosis. In addition, compound **7q** efficiently reduced the levels of Gal-1 protein in dose-dependent manner confirmed by ELISA. we have explored the feasibility of radiolabeling with ^{18}F radionuclide as to show that this cytotoxic molecule **7q** can also be used as a PET tracer in low concentration. Our studies show the potential of novel 4, 7-disubstituted coumarin derivatives in the development of a novel class of small molecules against oncogenesis.

4.0 Methods and Materials:

4.1 Chemistry

All the starting materials, specific reagents and solvents were purchased from commercial suppliers and utilized without further purification. Analytical thin layer chromatography (TLC) was performed on MERCK pre-coated silica gel 60-F254 aluminum plates. Visualization of the spots on TLC plates was achieved by exposure to iodine vapour and UV light. All melting points were recorded on Stuart® SMP30 melting point apparatus and are uncorrected. Column chromatography was performed using silica gel (60-120 mesh) and was eluted with ethyl acetate-hexane. NMR spectra were recorded on Bruker 500 (500 MHz for ^{1}H-NMR and 125 MHz for ^{13}C NMR) using $CDCl_3$ and DMSO as solvents. Chemical shift was reported in parts per million (ppm) with respect to internal standard Tetra Methyl Silane (TMS). Coupling constants were quoted in Hertz (Hz). High Resolution Mass Spectra

(HRMS) were obtained on Agilent Q-TOF-Mass Spectrometer 6540-UHD LC/HRMS operating at 70 eV using direct inlet.

4.1.1. Synthetic procedures and spectral data

4.1.1.1. Synthesis of 4-(chloromethyl)-7-hydroxy-2H-chromen-2-one **(3)**

A 50 mL round bottom flask was charged with resorcinol (1 equi) and ethyl-4-chloroacetoacetate (1.1 equi), make it into a clear solution than the solution was added drop wise to an externally cooled conc. H_2SO_4 (10 mL) contains in a 50 mL beaker at 10 °C and the reaction mixture was then stirred at room temperature for 20 min. After confirmation by TLC, the mixture was poured into ice water contained in a beaker, the precipitate compound **3** obtained was collected by suction filtration and washed with cold water, dried and recrystallized from ethanol. white solid, yield 91%; mp 186-188 °C; ^{1}H NMR (500 MHz, DMSO) δ 10.66 (s, 1H), 7.68 (d, J = 7.8 Hz, 1H), 6.90 – 6.71 (m, 2H), 6.42 (s, 1H), 4.96 (s, 2H). ^{13}C NMR (126 MHz, DMSO) δ 161.94, 160.61, 155.78, 151.45, 127.01, 113.55, 111.54, 109.83, 103.00, 41.83. HRMS (ESI): m/z calcd for $C_{10}H_7ClO_3$, 210.0084, found 211.0157 $[M+H]^+$

4.1.1.2. Synthesis of 7-hydroxy-4-(substituted morpholinomethyl)-2H-chromen-2-ones **(4a, 4b)**

To a solution of 4-(chloromethyl)-7-hydroxy-2H-chromen-2-one (1 mmol) **(3)** in freshly distilled acetone (5 mL), the substituted morpholines (1 mmol) and anhydrous K_2CO_3 (2.5 mmol) were added and the reaction mixture was stirred under reflux for 4-5 hr. After confirmation by TLC, solvent in the reaction mixture was removed by evaporation and left out crude solid residue was extracted with ethyl acetate (3x20 ml), dried over Na_2SO_4. The combined organic layer was concentrated in vacuo and the residues were purified by column chromatography on silica gel.

4.1.1.2.1. 7-hydroxy-4-(morpholinomethyl)-2H-chromen-2-one **(4a)**

white solid, yield 86%; mp 193-195 °C; ^{1}H NMR (500 MHz, DMSO) δ 10.56 (s, 1H), 7.80 (d, J = 6.9 Hz, 1H), 6.84 (dd, J = 8.7, 2.4 Hz, 1H), 6.76 (d, J = 2.4 Hz, 1H), 6.29 (s, 1H), 3.66 (s, 2H), 3.66 – 3.62 (t, J = 5.9 Hz, 4H), 2.51 (s, 4H). ^{13}C NMR (126 MHz, DMSO) δ 161.52, 160.82, 155.69, 152.86, 127.21, 113.24, 111.35, 110.67, 102.65, 66.69, 58.76, 53.83. HRMS (ESI): m/z calcd for $C_{14}H_{15}NO_4$, 261.1001, found 262.1075 $[M+H]^+$

4.1.1.2.2. 4-((2,6-dimethylmorpholino) methyl)-7-hydroxy-2H-chromen-2-one **(4b)**

Off white solid, yield 84%; mp 216-218 °C; ^{1}H NMR (500 MHz, DMSO) δ 10.51 (s, 1H), 7.75 (d, J = 8.8 Hz, 1H), 6.78 (dd, J = 8.7, 2.4 Hz, 1H), 6.70 (d, J = 2.4 Hz, 1H), 6.23 (s, 1H), 3.59 – 3.54 (m, 4H), 2.76 (d, J = 10.3 Hz, 2H), 1.75 (t, J = 10.7 Hz, 2H), 1.04 (d, J = 6.3 Hz, 6H). ^{13}C NMR (126 MHz, DMSO) δ 161.51, 160.84, 155.70, 152.92, 127.28, 113.23, 111.38, 110.77, 102.64, 71.50, 59.51, 58.44, 19.36. HRMS (ESI): m/z calcd for $C_{16}H_{19}NO_4$, 289.1314, found 290.1396 $[M+H]^+$

4.1.1.3. Synthesis of 7-hydroxy-4-(substituted piperidinomethyl)-2H-chromen-2-ones **(5a, 5b)**

To a solution of 4-(chloromethyl)-7-hydroxy-2H-chromen-2-one (1 mmol) **(3)** in freshly distilled acetone (5 mL), the substituted piperidines (1 mmol) and anhydrous K_2CO_3 (2.5 mmol) were and the reaction mixture was stirred under reflux for 5-6 hr. After confirmation by TLC, solvent in the reaction mixture was removed by evaporation left a crude solid residue that was extracted with ethyl acetate (3x20 ml) and dried over Na_2SO_4. The combined organic layer was concentrated in vacuo and the residues were purified by column chromatography on silica gel.

4.1.1.3.1. 7-hydroxy-4-((4-methylpiperidin-1-yl) methyl)-2H-chromen-2-one **(5a)**

white solid, yield 83%; mp 144-146 °C; ^{1}H NMR (500 MHz, DMSO) δ 10.50 (s, 1H), 7.75 (d, *J* = 8.7 Hz, 1H), 6.78 (dd, *J* = 8.7, 2.1 Hz, 1H), 6.71 (d, *J* = 2.1 Hz, 1H), 6.20 (s, 1H), 3.58 (s, 2H), 2.83 (d, *J* = 11.2 Hz, 2H), 2.02 (dd, *J* = 19.6, 8.9 Hz, 2H), 1.58 (d, *J* = 12.1 Hz, 2H), 1.40-1.32 (m, 1H), 1.19 – 1.11 (m, 2H), 0.89 (d, *J* = 6.5 Hz, 3H). ^{13}C NMR (125 MHz, DMSO) δ 161.55, 160.93, 155.67, 153.80, 127.14, 113.23, 111.42, 110.22, 102.64, 58.88, 54.09, 34.48, 30.57, 22.20. HRMS (ESI): m/z calcd for $C_{16}H_{19}NO_3$, 273.1365, found 274.1439 $[M+H]^+$

4.1.1.3.2. ethyl 1-((7-hydroxy-2-oxo-2H-chromen-4-yl) methyl) piperidine-4-carboxylate **(5b)**

white solid, yield 80%; mp 162-164 °C; ^{1}H NMR (500 MHz, DMSO) δ 7.76 (d, J = 8.8 Hz, 1H), 6.79 (dd, J = 8.7, 2.3 Hz, 1H), 6.71 (d, J = 2.3 Hz, 1H), 6.21 (s, 1H), 4.07 (q, J = 7.1 Hz, 2H), 3.60 (s, 2H), 2.82 (d, J = 11.5 Hz, 2H), 2.32 (s, 1H), 2.13 (dd, J = 11.2, 9.3 Hz, 2H), 1.85 – 1.78 (m, 2H), 1.63 – 1.55 (m, 2H), 1.18 (t, J = 7.1 Hz, 3H). ^{13}C NMR (125 MHz, DMSO) δ 174.75, 161.55, 160.89, 155.67, 153.50, 127.18, 113.23, 111.37, 110.35, 102.64, 60.25, 58.68, 52.97, 40.49, 28.48, 14.55. HRMS (ESI): m/z calcd for $C_{18}H_{21}NO_5$, 331.1420, found 332.1496 $[M+H]^+$

4.1.1.4. Synthesis of 4-((3,4-dihydroisoquinolin-2(1H)-yl) methyl)-7-hydroxy-2H-chromen-2-one **(6a)**

To a solution of 4-(chloromethyl)-7-hydroxy-2H-chromen-2-one (1 mmol) **(3)** in freshly distilled acetone (5 mL), the tetrahydroisoquinoline (1 mmol) and anhydrous K_2CO_3 (2.5 mmol) were and the reaction mixture was stirred under reflux for 3-4 hr and remaining procedure is as similar as the synthesis of 4a, 4b compounds. Brown solid, yield 84%; mp 171-173 °C; 1H NMR (500 MHz, DMSO) δ 7.83 (d, J = 8.8 Hz, 1H), 7.20-7.10 (m, 4H), 6.85 – 6.78 (m, 1H), 6.75 (d, J = 6.3 Hz, 1H), 6.30 (s, 1H), 3.65 (s, 2H), 3.02 (t, J = 5.7 Hz, 1H), 2.88 – 2.75 (m, 5H). 13C NMR (125 MHz, DMSO) δ 162.24, 160.97, 155.83, 153.34, 134.96, 134.38, 129.40, 128.93, 127.24, 126.52, 125.97, 113.48, 111.07, 110.31, 102.70, 58.43, 55.95, 51.03, 29.13. HRMS (ESI): m/z calcd for $C_{19}H_{17}NO_3$, 307.1208, found 308.1287 $[M+H]^+$

4.1.2. General procedure for the synthesis of final compounds 7a-y.

To the individual solution of compounds **4a, 4b, 5a, 5b and 6a (**1 equi) in freshly distilled acetone (10 mL), added K_2CO_3 (2.5 equi) as base and various alkyl halides and aryl halides (1.1 equi) were added and stirred under reflux for 2-3 h. The solvent was evaporated completely and the obtained residue was extracted with ethyl acetate (3x20 ml) and dried over Na_2SO_4. The combined organic layer was concentrated in vacuo and the residues were purified by column chromatography on silica gel, offered the final target compounds **7a-y** with moderate to good yields.

4.1.3 Spectral data for final compounds 7a-7y

4.1.3.1 4-(morpholinomethyl)-7-((4-nitrobenzyl)oxy)-2H-chromen-2-one **(7a)**

Off white solid, yield 85%; mp 174-176 °C; 1H NMR (500 MHz, CDCl3) δ 8.30 – 8.25 (m, 2H), 7.81 (d, J = 8.8 Hz, 1H), 7.62 (d, J = 8.8 Hz, 2H), 6.94 (d, J = 9.2, 4.6 Hz, 1H), 6.88 (d, J = 2.5 Hz, 1H), 6.42 (s, 1H), 5.25 (s, 2H), 3.76 (s, 4H), 3.64 (s, 2H), 2.59 (s, 4H). 13C NMR (125 MHz, DMSO+ CDCl3) δ 161.15, 160.54, 159.57, 155.49, 147.56, 144.18, 128.31, 126.80, 123.84, 112.83, 112.47, 112.32, 102.08, 68.99, 66.44, 53.64, 30.97. HRMS (ESI): m/z calcd for $C_{21}H_{20}N_2O_6$, 396.1321, found 397.1396 $[M+H]^+$

4.1.3.2 2-((4-(morpholinomethyl)-2-oxo-2H-chromen-7-yl) oxy)acetonitrile **(7b)**

Off white solid, yield 84%; mp 164-166 °C; 1H NMR (500 MHz, CDCl3) δ 7.86 (d, J = 8.6 Hz, 1H), 6.98 – 6.91 (m, 2H), 6.44 (s, 1H), 4.85 (s, 2H), 3.74 (t, J = 9.1 Hz, 4H), 3.60 (s, 2H),

2.54 (t, J = 8.7 Hz, 4H). 13C NMR (125 MHz, CDCl3) δ 160.67, 158.89, 155.36, 151.22, 126.66, 114.32, 114.22, 113.51, 111.99, 102.45, 66.89, 59.61, 53.80, 53.49. HRMS (ESI): m/z calcd for $C_{16}H_{16}N_2O_4$, 300.1110, found 301.1394 $[M+H]^+$

4.1.3.3 4-(morpholinomethyl)-7-(prop-2-yn-1-yloxy)-2H-chromen-2-one **(7c)**

Brown solid, yield 82%; mp 117-119 °C; ^{1}H NMR (500 MHz, CDCl3) δ 7.78 (d, J = 8.8 Hz, 1H), 6.99 – 6.87 (m, 2H), 6.40 (s, 1H), 4.77 (d, J = 2.3 Hz, 2H), 3.73 (t, J = 8.8 Hz, 4H), 3.60 (s, 2H), 2.58 (t, J = 2.3 Hz, 1H), 2.55 (t, J = 3.8 Hz, 4H). 13C NMR (125 MHz, CDCl3) δ 161.19, 160.34, 155.42, 151.53, 125.97, 113.05, 112.74, 112.47, 102.12, 77.42, 76.53, 66.90, 59.53, 56.17, 53.82. HRMS (ESI): m/z calcd for $C_{17}H_{17}NO_4$, 299.1158, found 300.1235 $[M+H]^+$

4.1.3.4 7-((4-bromobenzyl)oxy)-4-(morpholinomethyl)-2H-chromen-2-one **(7d)**

White solid, yield 83%; mp 184-186 °C; 1H NMR (500 MHz, CDCl3) δ 7.76 (d, J = 8.9 Hz, 1H), 7.55 – 7.50 (m, 2H), 7.31 (d, J = 8.4 Hz, 2H), 6.93 – 6.85 (m, 2H), 6.39 (s, 1H), 5.08 (s, 2H), 3.74 (s, 4H), 3.60 (s, 2H), 2.55 (s, 4H). 13C NMR (125 MHz, CDCl3) δ 161.37, 161.03, 155.58, 134.85, 131.93, 129.11, 126.00, 122.37, 112.86, 112.71, 112.32, 101.94, 69.69, 66.83, 59.56, 53.80. HRMS (ESI): m/z calcd for $C_{21}H_{20}BrNO_4$, 429.0576, found 430.0652 $[M+H]^+$

4.1.3.5 7-(allyloxy)-4-(morpholinomethyl)-2H-chromen-2-one **(7e)**

Off white solid, yield 84%; mp 106-108 °C; 1H NMR (500 MHz, CDCl3) δ 7.75 (d, J = 8.8 Hz, 1H), 6.93 – 6.81 (m, 2H), 6.40 (s, 1H), 6.05 (s, 1H), 5.45 (dd, J = 17.3 Hz, 1H), 5.35 (dd, J = 16.7 Hz, 1H), 4.61 (d, J = 5.3 Hz, 2H), 3.76 (s, 4H), 3.62 (s, 2H), 2.57 (s, 4H). 13C NMR (125 MHz, CDCl3) δ 161.70, 161.12, 155.62, 132.14, 125.87, 118.58, 112.91, 112.35, 101.84, 69.27, 66.63, 58.95, 53.70. HRMS (ESI): m/z calcd for $C_{17}H_{19}NO_4$, 301.1314, found 302.1392 $[M+H]^+$

4.1.3.6 4-((2,6-dimethylmorpholino)methyl)-7-((4-nitrobenzyl)oxy)-2H-chrom en-2-one **(7f)**

White solid, yield 86%; mp 195-197 °C; 1H NMR (500 MHz, CDCl3) δ 8.34 – 8.22 (m, 2H), 7.80 (d, J = 8.8 Hz, 1H), 7.62 (d, J = 8.8 Hz, 2H), 7.00 – 6.81 (m, 2H), 6.40 (s, 1H), 5.24 (s, 2H), 3.71 (s, 2H), 3.58 (s, 2H), 2.76 (s, 2H), 1.90 (s, 2H), 1.16 (d, J = 6.3 Hz, 6H). 13C NMR (125 MHz, CDCl3) δ 163.36, 160.81, 155.58, 147.85, 143.12, 127.73, 126.31, 124.00, 112.95, 112.78, 112.63, 101.99, 69.06, 59.51, 59.24, 30.93, 18.98. HRMS (ESI): m/z calcd for $C_{23}H_{24}N_2O_6$, 424.1634, found 425.1715 $[M+H]^+$

4.1.3.7 2-((4-((2,6-dimethylmorpholino) methyl)-2-oxo-2H-chromen-7-yl) oxy) acetonitrile **(7g)**

Off white solid, yield 83%; mp 146-148 °C; 1H NMR (500 MHz, CDCl3) δ 7.89 – 7.83 (m, 1H), 6.94 (dd, J = 7.3, 2.4 Hz, 2H), 6.43 (s, 1H), 4.86 (s, 2H), 3.70 (m, 2H), 3.57 (s, 2H), 2.73 (d, J = 10.4 Hz, 2H), 1.89 (t, J = 10.7 Hz, 2H), 1.16 (d, J = 6.3 Hz, 6H). 13C NMR (125 MHz, CDCl3) δ 160.74, 158.89, 155.34, 151.43, 126.72, 114.34, 114.27, 113.48, 112.02, 102.41, 71.66, 59.52, 59.22, 53.51, 30.93, 19.01. HRMS (ESI): m/z calcd for $C_{18}H_{20}N_2O_4$, 328.1423, found 329.1502 $[M+H]^+$

4.1.3.8 4-((2,6-dimethylmorpholino) methyl)-7-(prop-2-yn-1-yloxy)-2H-chrom en-2-one **(7h)**

Off white solid, yield 82%; mp 112-114 °C; 1H NMR (500 MHz, CDCl3) δ 7.78 (d, J = 7.2 Hz,1H), 6.98 – 6.87 (m, 2H), 6.39 (s, 1H), 4.77 (d, J = 2.2 Hz, 2H), 3.75 – 3.65 (m, 2H), 3.54 (d, J = 18.9 Hz, 2H), 2.74 (d, J = 10.6 Hz, 2H), 2.58 (t, J = 2.3 Hz, 1H), 1.88 (t, J = 10.6 Hz, 2H), 1.16 (d, J = 6.3 Hz, 6H). 13C NMR (125 MHz, CDCl3) δ 161.26, 160.32, 155.42, 151.74, 126.04, 113.10, 112.73, 112.47, 102.09, 77.43, 76.52, 71.68, 59.57, 59.16, 56.16, 19.02. HRMS (ESI): m/z calcd for $C_{19}H_{21}NO_4$, 327.1471, found 328.1548 $[M+H]^+$

4.1.3.9 4-(((4-((2,6-dimethylmorpholino) methyl)-2-oxo-2H-chromen-7-yl)oxy) methyl) benzonitrile **(7i)**

white solid, yield 83%; mp 180-182 °C; 1H NMR (500 MHz, CDCl3) δ 7.78 (d, J = 8.8 Hz, 1H), 7.71 (d, J = 8.2 Hz, 2H), 7.55 (d, J = 8.1 Hz, 2H), 6.94 – 6.84 (m, 2H), 6.39 (s, 1H), 5.19 (s, 2H), 3.71 (s, 2H), 3.57 (s, 2H), 2.75 (d, J = 10.1 Hz, 2H), 1.89 (t, J = 9.6 Hz, 2H), 1.16 (d, J = 6.3 Hz, 6H). 13C NMR (125 MHz, CDCl3) δ 155.58, 141.17, 132.58, 127.65, 126.26, 118.47, 112.80, 112.23, 101.99, 71.31, 69.30, 59.04, 30.93, 18.96. HRMS (ESI): m/z calcd for $C_{24}H_{24}N_2O_4$, 404.1736, found 405.1811 $[M+H]^+$

4.1.3.10 7-(allyloxy)-4-((2,6-dimethylmorpholino) methyl)-2H-chromen-2-one **(7j)**

Off white solid, yield 82%; mp 108-110 °C; 1H NMR (500 MHz, CDCl3) δ 7.75 (d, J = 9.6 Hz, 1H), 6.91 – 6.78 (m, 2H), 6.37 (s, 1H), 6.05 (m, 1H), 5.45 (dd, J = 17.3, 1.3 Hz, 1H), 5.35 (dd, J = 10.5, 1.2 Hz, 1H), 4.61 (d, J = 5.3 Hz, 2H), 3.75 – 3.65 (m, 2H), 3.54 (s, 2H), 2.74 (d, J = 10.7 Hz, 2H), 1.88 (t, J = 10.6 Hz, 2H), 1.16 (d, J = 6.3 Hz, 6H). 13C NMR (125 MHz, CDCl3) δ 161.62, 161.31, 155.60, 132.16, 125.91, 118.56, 112.86, 112.43, 101.77, 71.52, 69.25, 59.41, 58.92, 30.93, 18.99. HRMS (ESI): m/z calcd for $C_{19}H_{23}NO_4$, 329.1627, found 330.1704 $[M+H]^+$

4.1.3.11 4-((4-methylpiperidin-1-yl) methyl)-7-((4-nitrobenzyl) oxy)-2H-chrom en-2-one **(7k)**

Off white solid, yield 86%; mp 198-200 °C; 1H NMR (500 MHz, CDCl3) δ 8.32 – 8.23 (m, 2H), 7.86 (d, J = 8.2 Hz, 1H), 7.62 (d, J = 8.8 Hz, 2H), 6.94 (d, J = 8.7 Hz, 1H), 6.87 (d, J = 2.5 Hz, 1H), 6.43 (s, 1H), 5.24 (s, 2H), 3.65 (s, 2H), 2.95 (s, 2H), 2.17 (s, 2H), 1.65 (s, 2H), 1.42 (s, 3H), 0.95 (d, J = 5.5 Hz, 3H). 13C NMR (125 MHz, CDCl3) δ 161.16, 160.82, 155.51, 147.84, 144.01, 143.23, 127.71, 126.39, 123.99, 113.35, 112.62, 101.91, 69.02, 54.33, 33.81, 30.43, 21.71. HRMS (ESI): m/z calcd for $C_{23}H_{24}N_2O_5$, 408.1685, found 409.1763 $[M+H]^+$

4.1.3.12 2-((4-((4-methylpiperidin-1-yl) methyl)-2-oxo-2H-chromen-7-yl) oxy) acetonitrile **(7l)**

Off white solid, yield 83%; mp 152-154 °C; 1H NMR (500 MHz, CDCl3) δ 7.92 (d, J = 8.6 Hz, 1H), 6.98 – 6.90 (m, 2H), 6.46 (s, 1H), 4.85 (s, 2H), 3.63 (s, 2H), 2.95 (s, 2H), 2.24 – 2.05 (s, 2H), 1.64 (s, 2H), 1.48 – 1.22 (m, 3H), 0.94 (d, J = 6.2 Hz, 3H). 13C NMR (125 MHz, CDCl3) δ 160.87, 158.81, 155.28, 126.83, 114.55, 114.31, 113.35, 111.88, 102.39, 59.52, 54.34, 53.51, 34.17, 30.47, 21.75. HRMS (ESI): m/z calcd for $C_{18}H_{20}N_2O_3$, 312.1474, found 313.1550 $[M+H]^+$

4.1.3.13 4-(((4-((4-methylpiperidin-1-yl) methyl)-2-oxo-2H-chromen-7-yl)oxy) methyl)benzonitrile **(7m)**

Off white solid, yield 84%; mp 177-179 °C; ^{1}H NMR (500 MHz, CDCl3) δ 7.83 (d, J = 8.7 Hz, 1H), 7.70 (d, J = 8.2 Hz, 2H), 7.56 (d, J = 8.2 Hz, 2H), 6.95 – 6.82 (m, 2H), 6.40 (s, 1H), 5.19 (s, 2H), 3.59 (s, 2H), 2.90 (s, 2H), 2.14 (d, J = 28.0 Hz, 2H), 1.63 (s, 2H), 1.45 – 1.26 (m, 3H), 0.94 (d, J = 6.1 Hz, 3H). 13C NMR (125 MHz, CDCl3) δ 160.99, 155.52, 141.25, 132.58, 127.65, 126.39, 118.50, 113.00, 112.69, 112.19, 101.94, 69.28, 58.95, 54.26, 33.81, 30.27, 21.60. HRMS (ESI): m/z calcd for $C_{24}H_{24}N_2O_3$, 388.1787, found 389.1864 $[M+H]^+$

4.1.3.14 7-(allyloxy)-4-((4-methylpiperidin-1-yl) methyl)-2H-chromen-2-one **(7n)**

Brown solid, yield 82%; mp 107-109 °C; ^{1}H NMR (500 MHz, $CDCl_3$) δ 7.71 (d, *J* = 8.8 Hz, 1H), 6.83 – 6.71 (m, 2H), 6.31 (s, 1H), 5.98 (m, 1H), 5.37 (dd, *J* = 17.3, 1.4 Hz, 1H), 5.27 (dd, *J* = 10.5, 1.2 Hz, 1H), 4.53 (d, *J* = 5.3 Hz, 2H), 3.53 (s, 2H), 2.84 (s, 2H), 2.08 (s, 2H), 1.55 (s, 2H), 1.37 – 1.20 (m, 3H), 0.87 (d, *J* = 6.3 Hz, 3H). 13C NMR (125 MHz, CDCl3) δ 161.52, 161.43, 155.54, 132.22, 125.98, 118.51, 112.76, 112.65, 101.75, 69.22, 59.23, 54.30,

33.99, 30.40, 21.70. HRMS (ESI): m/z calcd for $C_{19}H_{23}NO_3$, 313.1678, found 314.1753 $[M+H]^+$

4.1.3.15 7-((4-bromobenzyl)oxy)-4-((4-methylpiperidin-1-yl)methyl)-2H-chrom en-2-one **(7o)**

white solid, yield 84%; mp 149-151 °C; 1H NMR (500 MHz, CDCl3) δ 7.81 (d, J = 8.8 Hz, 1H), 7.56 – 7.50 (m, 2H), 7.30 (d, J = 9.8 Hz, 2H), 6.94 – 6.83 (m, 2H), 6.40 (s, 1H), 5.08 (s, 2H), 3.63 (s, 2H), 2.93 (s, 2H), 2.16 (s, 2H), 1.64 (s, 2H), 1.33 (m, 3H), 0.94 (d, J = 5.9 Hz, 3H). 13C NMR (125 MHz, CDCl3) δ 161.41, 161.15, 155.53, 134.85, 131.92, 131.92, 129.12, 126.19, 122.36, 112.88, 102.01, 69.69, 54.22, 33.88, 30.25, 21.59. HRMS (ESI): m/z calcd for $C_{23}H_{24}BrNO_3$, 442.3530, found 444.0997 $[M+2]^+$

4.1.3.16 ethyl 1-((7-(benzyloxy)-2-oxo-2H-chromen-4-yl)methyl)piperidine-4-carboxylate **(7p)**

Brown solid, yield 84%; mp 130-132 °C; 1H NMR (500 MHz, CDCl3) δ 8.28 – 8.21 (m, 2H), 7.84 (d, J = 8.8 Hz, 1H), 7.67 – 7.52 (m, 3H), 6.96 – 6.82 (m, 2H), 6.38 (s, 1H), 5.24 (s, 2H), 4.14 (q, J = 7.1 Hz, 2H), 3.60 (s, 2H), 2.97 – 2.79 (m, 2H), 2.34 (s, 1H), 2.24 – 2.14 (m, 2H), 1.93 (s, 2H), 1.82 (s, 2H), 1.26 (t, J = 7.1 Hz, 3H). 13C NMR (125 MHz, CDCl3) δ 160.81, 155.54, 147.83, 143.15, 129.93, 127.73, 126.46, 126.20, 124.05, 124.00, 112.83, 112.74, 102.07, 69.05, 60.60, 52.93, 30.92, 29.69, 14.20. HRMS (ESI): m/z calcd for $C_{25}H_{27}NO_5$, 421.1889, found 422.1966 $[M+H]^+$

4.1.3.17 ethyl 1-((7-((4-nitrobenzyl) oxy)-2-oxo-2H-chromen-4-yl)methyl) piperidine-4-carboxylate **(7q)**

Brown solid, yield 86%; mp 135-137 °C; 1H NMR (500 MHz, CDCl3) δ 7.77 (d, J = 8.8 Hz, 1H), 7.42 (m, 3H), 7.35 (m, 1H), 6.93 – 6.87 (m, 2H), 6.34 (s, 1H), 5.13 (s, 2H), 4.14 (q, J = 7.1 Hz, 2H), 3.56 (s, 2H), 2.87 (d, J = 11.4 Hz, 2H), 2.31 (m, 1H), 2.20 – 2.11 (m, 2H), 1.94 – 1.86 (m, 2H), 1.82 – 1.74 (m, 2H), 1.25 (t, J = 6.6 Hz, 3H). 13C NMR (125 MHz, CDCl3) δ 174.98, 161.59, 161.48, 155.55, 152.38, 135.88, 128.76, 128.36, 127.51, 126.06, 112.84, 111.92, 101.87, 70.45, 60.41, 53.30, 40.85, 30.92, 28.27, 14.22. HRMS (ESI): m/z calcd for $C_{25}H_{26}N_2O_7$, 466.1740, found 467.1818 $[M+H]^+$

4.1.3.18 ethyl 1-((7-((4-bromobenzyl) oxy)-2-oxo-2H-chromen-4-yl) methyl) piperidine-4-carboxylate **(7r)**

Off white solid, yield 81%; mp 127-129 °C; ^{1}H NMR (500 MHz, $CDCl_3$) δ 7.82 (d, *J* = 8.8 Hz, 1H), 7.53 (d, *J* = 8.3 Hz, 2H), 7.31 (d, *J* = 8.3 Hz, 2H), 6.94 – 6.85 (m, 2H), 6.42 (s, 1H), 5.09 (d, *J* = 13.3 Hz, 2H), 4.14 (q, *J* = 7.1 Hz, 2H), 3.69 (s, 2H), 2.95 (s, 2H), 2.38 (s, 2H), 2.17 (s, 1H), 1.99 (s, 2H), 1.83 (s, 2H), 1.26 (t, *J* = 7.1 Hz, 3H). 13C NMR (125 MHz, CDCl3) δ 161.53, 155.55, 134.82, 131.92, 129.12, 126.20, 122.36, 112.91, 112.66, 102.05, 69.70, 60.59, 52.94, 30.92, 28.14, 14.20. HRMS (ESI): m/z calcd for $C_{25}H_{26}N_2O_7$, 500.3890, found 502.1053 $[M+2]^+$

4.1.3.19 ethyl 1-((7-((4-methoxybenzyl) oxy)-2-oxo-2H-chromen-4-yl) methyl) piperidine-4-carboxylate **(7s)**

Brown solid, yield 80%; mp 105-107 °C; 1H NMR (500 MHz, CDCl3) δ 7.76 (d, J = 9.2 Hz, 1H), 7.36 (d, J = 8.6 Hz, 2H), 6.93 (d, J = 8.6 Hz, 2H), 6.90 – 6.87 (m, 2H), 6.34 (s, 1H), 5.05 (s, 2H), 4.14 (q, J = 7.1 Hz, 2H), 3.82 (s, 3H), 3.54 (d, J = 19.1 Hz, 2H), 2.88 (d, J = 11.4 Hz, 2H), 2.35 – 2.28 (m, 1H), 2.20 – 2.14 (m, 2H), 1.91 (d, J = 11.2 Hz, 2H), 1.80 (d, J = 17.7, 6.8 Hz, 2H), 1.25 (d, J = 6.8 Hz, 3H). 13C NMR (125 MHz, CDCl3) δ 174.95, 161.69, 161.50, 159.74, 155.55, 129.33, 127.86, 126.01, 114.18, 113.80, 112.91, 112.61, 111.88, 101.83, 70.28, 60.41, 55.33, 53.27, 40.81, 30.91, 28.24, 14.21. HRMS (ESI): m/z calcd for $C_{26}H_{29}NO_6$, 451.1995, found 452.2069 $[M+H]^+$

4.1.3.20 ethyl 1-((7-((4-cyanobenzyl) oxy)-2-oxo-2H-chromen-4-yl) methyl) piperidine-4-carboxylate **(7t)**

white solid, yield 84%; mp 149-151 °C; ^{1}H NMR (500 MHz, $CDCl_3$) δ 7.84 (d, *J* = 8.2 Hz, 1H), 7.71 (d, *J* = 8.1 Hz, 2H), 7.56 (d, *J* = 8.1 Hz, 2H), 6.89 (m, 2H), 6.39 (s, 1H), 5.19 (s, 2H), 4.14 (q, *J* = 7.1 Hz, 2H), 3.61 (s, 2H), 2.94 (d, *J* = 22.8 Hz, 2H), 2.34 (s, 1H), 2.17 (s, 2H), 1.93 (s, 2H), 1.83 (s, 2H), 1.26 (t, *J* = 7.0 Hz, 3H). 13C NMR (125 MHz, CDCl3) δ 160.80, 155.51, 147.82, 143.13, 129.90, 127.71, 126.42, 126.22, 124.03, 124.01, 112.80, 112.71, 102.09, 69.04, 60.61, 52.92, 30.94, 29.67, 14.24. HRMS (ESI): m/z calcd for $C_{26}H_{26}N_2O_5$, 446.1842, found 447.1918 $[M+H]^+$

4.1.3.21 4-((3,4-dihydroisoquinolin-2(1H)-yl) methyl)-7-((4-nitrobenzyl) oxy)-2H-chromen-2-one **(7u)**

Brown solid, yield 85%; mp 190-192 °C; ^{1}H NMR (500 MHz, $CDCl_3$) δ 8.26 (d, *J* = 8.7 Hz, 2H), 7.89 (d, *J* = 8.8 Hz, 1H), 7.61 (d, *J* = 8.7 Hz, 2H), 7.16 (m, 3H), 7.02 (d, *J* = 7.0 Hz, 1H), 6.93 – 6.86 (m, 2H), 6.49 (s, 1H), 5.23 (s, 2H), 3.88 (d, *J* = 25.2 Hz, 4H), 2.99 (s, 4H). 13C NMR (125 MHz, CDCl3) δ 161.05, 160.95, 155.56, 147.81, 143.21, 133.46, 128.77,

127.72, 126.64, 126.59, 125.99, 123.99, 113.05, 112.72, 102.00, 69.02, 58.60, 55.87, 50.91, 28.62. HRMS (ESI): m/z calcd for $C_{26}H_{22}N_2O5$, 442.1529, found 443.1594 $[M+H]^+$

4.1.3.22 7-((4-bromobenzyl) oxy)-4-((3,4-dihydroisoquinolin-2(1H)-yl) methyl)-2H-chromen-2-one **(7v)**

Pale brown solid, yield 80%; mp 168-170 °C; ^{1}H NMR (500 MHz, $CDCl_3$) δ 7.84 (d, *J* = 8.5 Hz, 1H), 7.51 (d, *J* = 8.3 Hz, 2H), 7.30 (d, *J* = 8.3 Hz, 2H), 7.19 – 7.11 (m, 3H), 7.01 (d, *J* = 6.7 Hz, 1H), 6.90 – 6.85 (m, 2H), 6.45 (s, 1H), 5.07 (s, 2H), 3.82 (d, *J* = 20.0 Hz, 4H), 2.98 – 2.88 (m, 4H). 13C NMR (125 MHz, CDCl3) δ 161.37, 161.29, 155.56, 152.13, 134.90, 134.16, 134.03, 131.91, 129.12, 128.74, 126.53, 126.39, 126.36, 125.80, 122.33, 112.87, 112.81, 112.33, 101.88, 69.65, 59.19, 56.25, 51.00, 29.07. HRMS (ESI): m/z calcd for $C_{26}H_{22}BrNO_3$, 475.0783, found 476.0860 $[M+H]^+$

4.1.3.23 4-((4-((3,4-dihydroisoquinolin-2(1H)-yl) methyl)-2-oxo-2H-chromen-7-yl) oxy) methyl) benzonitrile **(7w)**

Brown solid, yield 82%; mp 197-199 °C; 1H NMR (500 MHz, CDCl3) δ 7.89 (d, J = 8.8 Hz, 1H), 7.70 (d, J = 8.2 Hz, 2H), 7.55 (d, J = 8.4 Hz, 2H), 7.22 – 7.14 (m, 3H), 7.02 (d, J = 7.3 Hz, 1H), 6.90 (m, 2H), 6.51 (s, 1H), 5.19 (s, 2H), 3.94 (s, 4H), 3.02 (s, 4H). 13C NMR (125 MHz, CDCl3) δ 161.15, 160.95, 155.54, 141.32, 133.83, 132.60, 132.55, 128.79, 127.67, 127.63, 126.54, 125.94, 118.55, 113.11, 112.73, 112.19, 101.96, 69.30, 58.96, 56.10, 51.00, 28.89. HRMS (ESI): m/z calcd for $C_{27}H_{22}N_2O_3$, 422.1630, found 423.1708 $[M+H]^+$

4.1.3.24 2-((4-((3,4-dihydroisoquinolin-2(1H)-yl) methyl)-2-oxo-2H-chromen-7-yl) oxy) acetonitrile **(7x)**

Brown solid, yield 81%; mp 135-137 °C; 1H NMR (500 MHz, CDCl3) δ 7.95 (d, J = 8.8 Hz, 1H), 7.18 – 7.11 (m, 3H), 7.02 (d, J = 6.6 Hz, 1H), 6.92 (m, 2H), 6.50 (s, 1H), 4.84 (s, 2H), 3.84 – 3.77 (m, 4H), 2.97 – 2.86 (m, 4H). 13C NMR (125 MHz, CDCl3) δ 160.79, 158.89, 155.36, 151.75, 134.00, 133.94, 128.75, 127.00, 126.53, 126.46, 125.85, 114.42, 114.27, 113.55, 112.00, 102.39, 59.19, 56.20, 53.50, 50.99, 29.02. HRMS (ESI): m/z calcd for $C_{21}H_{18}N_2O_3$, 346.1317, found 347.1393 $[M+H]^+$

4.1.3.25 7-(allyloxy)-4-((3,4-dihydroisoquinolin-2(1H)-yl) methyl)-2H-chromen -2-one **(7y)**

Pale brown solid, yield 82%; mp 102-104 °C; ^{1}H NMR (500 MHz, $CDCl_3$) δ 7.83 (d, *J* = 8.7 Hz, 1H), 7.18 (m, 3H), 7.02 (d, *J* = 7.2 Hz, 1H), 6.85 (m, 2H), 6.49 (s, 1H), 6.04 (m, 1H), 5.44 (dd, *J* = 17.3, 1.2 Hz, 1H), 5.35 (d, *J* = 16.3, 1.2 Hz, 1H), 4.60 (d, *J* = 5.3 Hz, 2H), 3.93

(s, 4H), 3.03 (s, 4H). 13C NMR (125 MHz, CDCl3) δ 161.65, 161.25, 155.62, 133.62, 132.19, 128.75, 126.59, 126.17, 125.99, 118.53, 112.85, 112.68, 112.45, 101.83, 69.24, 58.32, 55.87, 50.88, 28.78. HRMS (ESI): m/z calcd for $C_{22}H_{21}NO_3$, 347.1521, found 348.1599 $[M+H]^+$

4.2. Radiochemistry

4.2.1 General Procedure:

All the chemicals and reagents were procured from Loba chemie (Mumbai, INDIA). The quality control was performed using various instruments like Gas chromatography (Scion 436 GC, Netherlands) having flame ionization detector (FID), Thin layer chromatography (TLC) scanner (EZ-SCAN, California, USA) with multimode radiation detector (OMNI-RAD, California. USA), Dose calibrator (Capintec CRC-25PET, New Jersey. USA), High performance liquid chromatography (HPLC) system (Dionex, ICS- 5000+, +, California. USA), pH paper (Fisher Scientific, New Hampshire. USA). The [^{18}F] radioisotopes were produced with 16.5MeV in-house Cyclotron (PETtrace 860, GE Healthcare, USA) by the proton bombardment on the enriched O-18 water using ^{18}O (p, n) ^{18}F reaction. The proton bombardment was done with the beam current of range of 30 µA -65 µA for 10 min depending upon the requirement of [^{18}F]. For the radiolabeling, the produced [18F] was delivered to semiautomatic synthesizer module (Tracerlab FX2N, GE Healthcare, Chicago. USA) using the Helium (UHP-5.5) as a carrier gas.

4.2.2 Radio synthesis of target compound

A stock solution for [^{18}F] eluent was prepared by dissolving 60 mg of Kryptofix (K222) and 12 mg of potassium carbonate in 12.0 ml of acetonitrile along with 525 µL of the deionized water. The [^{18}F] was eluted from conditioned QMA cartridge with a mixture of QMA eluent stock solution (1.5 mL) and acetonitrile (0.5 mL) into the reactor. Initially, complex of [K 2.2.2] K+[^{18}F]- was dried and, the reaction with the precursor (4±0.5 mg,) in 1.5 ml of DMF (**3**) was carried out at 160°C for 30 min. After completion of the reaction, the reaction mixture was diluted with acidic water (6 mL, pH=3.0) and passed through tC18 light cartridge for primary purification. The cartridge was washed with 4 mL of water, and 3 mL of 8% ethanol. The final purification was performed using 3 mL of 20-100% ethanol.

4.2.3.-Quality control parameters

The radiochemical purity of the preparation was estimated by thin-layer chromatography (TLC) and high-performance liquid chromatography (HPLC).

a) TLC parameters, around 3-5 µL of each sample was spotted on silica gel TLC sheet just 0.5 cm above the bottom and run the TLC using acetonitrile/saline (1:1) the following suitable solvent system.

a) HPLC parameters

The mobile phase was run in a gradient method for better resolution of peaks on the spectra. The acetonitrile (ACN) (solvent A) and water (solvent B) are used in different proportions. The gradient method was started with 5% acetonitrile (0-5 min), 5% to 100% acetonitrile (5-20 min), then100% acetonitrile (20-25 min) and again at 5% acetonitrile (25-30min). The stationary phase was the C18 column (250 mm X 4.6 mm, 5 µm), and UV detection wavelength (λ_{max}) was 280 nm with a flow rate of 1 mL/min.

c) **Residual solvent analysis**

The residual analysis was performed using gas chromatography. 1.0 µL of the sample was injected into the injector and analysis was started. The column was operated initially at 40°C for the first 3 min and then rise 50°C/min up to 8 min and the final temperature was set at 240°C and the column was BR-200ms, 0.32 mm ID. The makeup gas consists of Helium (28 mL/min), zero air (300 mL/min) and hydrogen gas (30 mL/min) flow at the rate of 2 mL/min.

4.3 Biology:

4.3.1 Maintenance of cell culture and cell proliferation assay:

All the cell lines were procured from ATCC (American Type Culture Collection, USA). Cells were grown in DMEM (Dulbecco's modified Eagle's medium) with 10% fetal bovine serum. Cell was maintained in a humidified incubator with 5% CO2 at 37^{o}C. For the anti-cytotoxicity assay, cells were seeded at a density of 10,000 cells/well and treated with conjugates for 72 h. Further, cells were fixed with 10% Trichloroacetic acid for 1hour at 4 ^{o}C and washed with running tap water. 100µl of 0.057% of sulphorhodamine B was added per well and incubated for 30mins and further washed with 1% acetic acid to remove the unbound dye. To elute the dye, 10mM Tris having pH 10.5 was added and reading was captured at 510nm with Varioskan Flash spectral scanning multimode reader.

4.3.2 Quantikine ELISA Human Gal-1 Immunoassay

This assay utilizes the quantitative sandwich enzyme immunoassay technique. The assay was performed as per the protocol of quantitative enzyme immunoassay manufacture's (R & D human galectins quantikine ELISA kit, USA).

4.3.3 Fluorescence measurements

In order to perform fluorescence binding studies of Gal-1 with compound 7q, full-length ORF of Gal-1 was cloned into pET28a expression vector followed by purification using Ni-NTA affinity chromatography as reported by Hsieh and co-authors, 2015 [38]. Intrinsic fluorescence measurements were carried out on a Jasco spectrofluorimeter equipped with Peltier at 25°C. Compound 7q was dissolved in DMSO to prepare a stock of 10 mM and was used in the range of 0-65 µM. Purified Gal-1with concentration of 13 µM in 10 mM phosphate buffer (pH 7.5) was excited at 280 nm and the emission was recorded from 300-400 nm using a cuvette of 10 mm path length. Slit width 5 nm was used for excitation and emission, while scan speed was maintained at 100 nm/min. Buffer correction was made for each spectrum. Binding constant (K_a) and number of binding sites (n) were determined using modified Stern-Volmer equation i.e. $\log(F_o\text{-}F)/F = \log K_a + n\log[Q]$ where F_o and F is the intensity of the protein in the absence and presence of the ligand respectively, whereas n is the number of binding sites and Q is the ligand concentration.

4.3.4 Cell cycle analysis:

For analysis of cell cycle distribution, cells were seeded in 60mm culture dishes and treated with conjugate for 48 h. Post-treatment, cells were trypsinized, washed with phosphate buffer saline (PBS) and fixed with 70% ethanol overnight. On the day of analysis, cells were washed with PBS and incubated at 37oC for 30 minutes in a staining solution containing propidium iodide and triton x-100. Post-incubation, cells were washed and analyzed with BD Accuri C6 flow cytometer. The sample analysis was processed with FCSalyzer software.

4.3.5 Annexin-V Alexa Fluor 488 staining:

To evaluate the extent of apoptosis undergoing cells, Annexin-V Alexa 488/propidium iodide staining was employed. Staining was carried out as per manufacturer's protocol (#V13241, Invitrogen, USA). Briefly, cells were seeded in 60mm culture dishes and treated with conjugates for 48 h. Post-treatment, cells were stained with 5 µl of Annexin V Alexa Fluor

488 and 1µl of 100µg of Propidium Iodide (PI) for 15 minutes. Cells were then analyzed with the BD Accuri C6 flow cytometer and FCSalyzer software was used for analysis.

4.3.6 Acridine orange/Ethidium bromide staining:

Acridine orange/Ethidium staining reveals the extent of apoptosis undergoing cells in the treated versus untreated cells. Cells were seeded on coverslips and incubated for 48 h with the conjugate. Further, a staining solution containing 100µg/ml of acridine orange and 100µg/ml of Ethidium bromide was added to cells and incubated in dark at 37oC. Cells were imaged with a fluorescence inverted microscope (CKX41, Olympus, USA) at 10X magnification.

4.3.7 Hoechst 33342 staining:

To analyze the alterations in the nuclear architecture, PC-3 cells were seeded on cover slips and treatment with conjugate for 48 h. Cells were washed and fixed with 4% p-formaldehyde and incubated for 20 minutes. Plates were washed and stained with Hoechst 33342 (2µg/ml) for 5-10 minutes. Excess stain was washed with PBS and mounted on slides. Slides were analyzed under a fluorescent inverted microscope (Olympus, USA) at 10X magnification.

4.3.8 JC-1 staining:

For measuring the mitochondrial membrane potential, cells were seeded in 60mm culture dishes and treated with conjugates for 48 h. Further, cells were harvested with trypsin and stained with 10µg/ml of JC-1 (#PK-CA 707-7001, PromoKine, Germany) for 10minutes at 37 oC. Post-incubation, red and green fluorescence were measured by BD Accuri C6 flow cytometer and analysis with FCSalyzer was carried out.

4.3.9 H2DCFDA staining:

For the estimation of reactive oxygen species (ROS), H2DCFDA staining was employed. Cells seeded in 60mm dishes were treated with conjugates for 48 h. Cells were trypsinized and stained with carboxy-H2DCFDA for 30 minutes in dark at 37 oC. Images were captured with an Olympus fluorescence inverted microscope (CKX41) at 10X objective.

4.4 Molecular modeling studies

All computational calculations were performed on an Intel (R) Xenon(R) 2 Duo CPU E7600 @ 3.06GHz processor with the LINUX operating system. The software package used was the Schrodinger drug discovery consisting of modules for ligand, protein preparation and Glide for high-throughput virtual screening for docking. Protein preparation wizard was used to prepare Gal-1 downloaded from PDB (PDB ID: 4Y24), ready for docking i.e. removing waters, adding missing side chains and energy minimization by an OPLS-2005 force field. The final compound **7q** was sketched and converted to 3D using Ligprep. The Glide XP docking algorithm was employed using a grid box volume of 10x 10x 10 Å at the center of TD-139 as standard. A set of ADMET related properties were calculated using qikprop program i.e., Qikprop, version 6.5, Schrödinger, LLC, New York, NY, 2014.

Acknowledgments

1. Department of Biotechnology (DBT), Govt. of India, New Delhi for financial assistance (6242-19/RGCB/PMD/DBT/MLKA/2015).

2. National Institute of Pharmaceutical Education and Research (NIPER), Hyderabad for resources and facilities.

Conflict of Interest

Authors declare no conflicts

References:

[1] R.L. Siegel, K.D. Miller, A. Jemal, Cancer Statistics, 2017, CA Cancer J Clin. 67 (2017) 7–30.

[2] M. Mareel, A. Leroy, Clinical, cellular, and molecular aspects of cancer invasion, Physiol. Rev. 83 (2003) 337–376.

[3] D. Hanahan, R.A. Weinberg, Hallmarks of cancer: the next generation, Cell. 144 (2011) 646–674.

[4] M. Safavi, N. Esmati, S.K. Ardestani, S. Emami, S. Ajdari, J. Davoodi, A. Shafiee, A. Foroumadi, Halogenated flavanones as potential apoptosis-inducing agents: Synthesis and biological activity evaluation, European Journal of Medicinal Chemistry. 58 (2012) 573–580.

[5] L. Astorgues-Xerri, M.E. Riveiro, A. Tijeras-Raballand, M. Serova, C. Neuzillet, S. Albert, E. Raymond, S. Faivre, Unraveling galectin-1 as a novel therapeutic target for cancer, Cancer Treatment Reviews. 40 (2014) 307–319.

[6] I. Camby, M. Le Mercier, F. Lefranc, R. Kiss, Galectin-1: a small protein with major functions, Glycobiology. 16 (2006) 137R-157R.

[7] K. Wdowiak, T. Francuz, E. Gallego-Colon, N. Ruiz-Agamez, M. Kubeczko, I. Grochoła, J. Wojnar, Galectin Targeted Therapy in Oncology: Current Knowledge and Perspectives, International Journal of Molecular Sciences. 19 (2018) 210.

[8] G.A. Rabinovich, Galectin-1 as a potential cancer target, British Journal of Cancer. 92 (2005) 1188–1192.
[9] J. Cousin, M. Cloninger, The Role of Galectin-1 in Cancer Progression, and Synthetic Multivalent Systems for the Study of Galectin-1, International Journal of Molecular Sciences. 17 (2016) 1566.
[10] S. Vallabhajosula, 18F-Labeled Positron Emission Tomographic Radiopharmaceuticals in Oncology: An Overview of Radiochemistry and Mechanisms of Tumor Localization, Seminars in Nuclear Medicine. 37 (2007) 400–419.
[11] M.M. Alauddin, Positron emission tomography (PET) imaging with (18) F-based radiotracers, Am J Nucl Med Mol Imaging. 2 (2012) 55–76.
[12] X. Yu, X. Li, X. Song, D. Dai, L. Zhu, Y. Zhu, J. Wang, H. Zhao, W. Xu, Advantages and disadvantages of F-18 fluorodeoxyglucose positron emission tomography/computed tomography in carcinoma of unknown primary, Oncol Lett. 12 (2016) 3785–3792.
[13] A. Almuhaideb, N. Papathanasiou, J. Bomanji, 18F-FDG PET/CT imaging in oncology, Ann Saudi Med. 31 (2011) 3–13.
[14] V. Vassileva, S.M. Stribbling, C. Barnes, L. Carroll, M. Braga, J. Abrahams, K. Heinzmann, C. Haegeman, M. MacFarlane, K.L. Simpson, C. Dive, J. Honeychurch, T.M. Illidge, E.O. Aboagye, Evaluation of apoptosis imaging biomarkers in a genetic model of cell death, EJNMMI Res. 9 (2019) 18.
[15] A.K. Buck, S.N. Reske, Cellular origin and molecular mechanisms of 18F-FDG uptake: is there a contribution of the endothelium?, J. Nucl. Med. 45 (2004) 461–463.
[16] E. Kluza, I. Jacobs, S.J.C.G. Hectors, K.H. Mayo, A.W. Griffioen, G.J. Strijkers, K. Nicolay, Dual-targeting of αvβ3 and galectin-1 improves the specificity of paramagnetic/fluorescent liposomes to tumor endothelium in vivo, Journal of Controlled Release. 158 (2012) 207–214.
[17] X.-M. Peng, G. L.V. Damu, C.- He Zhou, Current Developments of Coumarin Compounds in Medicinal Chemistry, Current Pharmaceutical Design. 19 (2013) 3884–3930.
[18] S. Emami, S. Dadashpour, Current developments of coumarin-based anti-cancer agents in medicinal chemistry, European Journal of Medicinal Chemistry. 102 (2015) 611–630.
[19] M. Kaur, S. Kohli, S. Sandhu, Y. Bansal, G. Bansal, Coumarin: A Promising Scaffold for Anticancer Agents, Anti-Cancer Agents in Medicinal Chemistry. 15 (2015) 1032–1048.
[20] J. Dandriyal, R. Singla, M. Kumar, V. Jaitak, Recent developments of C-4 substituted coumarin derivatives as anticancer agents, European Journal of Medicinal Chemistry. 119 (2016) 141–168.
[21] N.S. Goud, S.M. Ghouse, J. Vishnu, J. Pranay, R. Alvala, V. Talla, I.A. Qureshi, M. Alvala, Synthesis and Biological Evaluation of Novel Heterocyclic Imines Linked Coumarin-Thiazole Hybrids as Anticancer Agents, ACAMC. 19 (2019).
[22] D. Cao, Y. Liu, W. Yan, C. Wang, P. Bai, T. Wang, M. Tang, X. Wang, Z. Yang, B. Ma, L. Ma, L. Lei, F. Wang, B. Xu, Y. Zhou, T. Yang, L. Chen, Design, Synthesis, and Evaluation of in Vitro and in Vivo Anticancer Activity of 4-Substituted Coumarins: A Novel Class of Potent Tubulin Polymerization Inhibitors, Journal of Medicinal Chemistry. 59 (2016) 5721–5739.

[23] V.K. Rajput, H. Leffler, U.J. Nilsson, B. Mukhopadhyay, Synthesis and evaluation of iminocoumaryl and coumaryl derivatized glycosides as galectin antagonists, Bioorganic & Medicinal Chemistry Letters. 24 (2014) 3516–3520.
[24] H. Zhao, A.C. Donnelly, B.R. Kusuma, G.E.L. Brandt, D. Brown, R.A. Rajewski, G. Vielhauer, J. Holzbeierlein, M.S. Cohen, B.S.J. Blagg, engineering an Antibiotic to Fight Cancer: Optimization of the Novobiocin Scaffold to Produce Anti-Proliferative Agents, Journal of Medicinal Chemistry. 54 (2011) 3839–3853.
[25] K. Benci, L. Mandić, T. Suhina, M. Sedić, M. Klobučar, S. Kraljević Pavelić, K. Pavelić, K. Wittine, M. Mintas, Novel Coumarin Derivatives Containing 1,2,4-Triazole, 4,5-Dicyanoimidazole and Purine Moieties: Synthesis and Evaluation of Their Cytostatic Activity, Molecules. 17 (2012) 11010–11025.
[26] D.S. Khachatryan, A.L. Razinov, A.V. Kolotaev, S.K. Belus̆, K.R. Matevosyan, Alkylation of NH-, OH-, and SH-acids in the presence of potassium carbonate: 1. Functionalization of chloromethyl group of alkoxy-substituted aromatic aldehydes, Russian Chemical Bulletin. 64 (2015) 395–404.
[27] H. Sun, S.G. DiMagno, Room-Temperature Nucleophilic Aromatic Fluorination: Experimental and Theoretical Studies, Angewandte Chemie International Edition. 45 (2006) 2720–2725.
[28] S.-S. Farn, Y.-H. Yeh, C.-C. Li, C.-S. Yang, J.-T. Chen, C.-S. Yu, W.-J. Lin, Development and validation of a reversed-phase HPLC method for analysis of radiochemical purity in [123 I] IBZM, Applied Radiation and Isotopes. 127 (2017) 61–67.
[29] S. Li, A. Schmitz, H. Lee, R.H. Mach, Automation of the Radiosynthesis of Six Different 18F-labeled radiotracers on the AllinOne, EJNMMI Radiopharmacy and Chemistry. 1 (2017).
[30] M. Mihon, C. Tuta, R. Leonte, A.C. Ion, V. Lavric, D. Niculae, An Improved Methodology for Determination of Radiochemical and Chemical Impurities in The Synthesis Process of 18f-Fdg (2-[18f] Fluoro-2-Deoxy-D-Glucose), Environmental Engineering and Management Journal. 14 (2015) 289–296.
[31] W.-A. Hsueh, A.L. Kesner, A. Gangloff, M.D. Pegram, M. Beryt, J. Czernin, M.E. Phelps, D.H.S. Silverman, Predicting chemotherapy response to paclitaxel with 18F-Fluoropaclitaxel and PET, J. Nucl. Med. 47 (2006) 1995–1999.
[32] O. Shamni, H. Grievink, B. Itamar, E. Mishani, G. Abourbeh, Development of a Fluorinated Analogue of Erlotinib for PET Imaging of EGFR Mutation–Positive NSCLC, Molecular Imaging and Biology. 21 (2019) 696–704.
[33] H. Su, Y. Seimbille, G.Z. Ferl, C. Bodenstein, B. Fueger, K.J. Kim, Y.-T. Hsu, S.M. Dubinett, M.E. Phelps, J. Czernin, W.A. Weber, Evaluation of [18F] gefitinib as a molecular imaging probe for the assessment of the epidermal growth factor receptor status in malignant tumors, European Journal of Nuclear Medicine and Molecular Imaging. 35 (2008) 1089–1099.
[34] P. Kumar, B. Singh, A. Ghai, P.P. Hazari, B.R. Mittal, A.K. Mishra, Development of a single vial kit formulation of [99mTc]-labeled doxorubicin for tumor imaging and treatment response assessment-preclinical evaluation and preliminary human results: [99mTc]-doxorubicin kit development for tumor imaging, Journal of Labelled Compounds and Radiopharmaceuticals. 58 (2015) 242–249.

[35] V. Vichai, K. Kirtikara, Sulforhodamine B colorimetric assay for cytotoxicity screening, Nature Protocols. 1 (2006) 1112–1116.
[36] D. Compagno, L.D. Gentilini, F.M. Jaworski, I.G. Perez, G. Contrufo, D.J. Laderach, Glycans and galectins in prostate cancer biology, angiogenesis and metastasis, Glycobiology. 24 (2014) 899–906.
[37] R. Wu, T. Wu, K. Wang, S. Luo, Z. Chen, M. Fan, D. Xue, H. Lu, Q. Zhuang, X. Xu, Prognostic significance of galectin-1 expression in patients with cancer: a meta-analysis, Cancer Cell Int. 18 (2018) 108.
[38] Lakowicz JR. Principles of Fluorescence Spectroscopy. third edition. *Springer US*. 2006.
[39] I. Vermes, C. Haanen, H. Steffens-Nakken, C. Reutellingsperger, A novel assay for apoptosis Flow cytometric detection of phosphatidylserine expression on early apoptotic cells using fluorescein labelled Annexin V, Journal of Immunological Methods. 184 (1995) 39–51.
[40] Baskić D, Popović S, Ristić P, Arsenijević NN. Analysis of cycloheximide-induced apoptosis in human leukocytes: fluorescence microscopy using annexin V/propidium iodide versus acridin orange/ethidium bromide. *Cell Biol Int*. 2006;30(11):924-932.
[41] Crowley LC, Marfell BJ, Waterhouse NJ. Analyzing Cell Death by Nuclear Staining with Hoechst 33342. *Cold Spring Harbor Protocols*. 2016;2016(9)
[42] Ly JD, Grubb DR, Lawen A. The mitochondrial membrane potential (deltapsi(m)) in apoptosis; an update. *Apoptosis*. 2003;8(2):115-128.
[43] Perelman A, Wachtel C, Cohen M, Haupt S, Shapiro H, Tzur A. JC-1: alternative excitation wavelengths facilitate mitochondrial membrane potential cytometry. *Cell Death & Disease*. 2012;3(11):1430-1430.
[44] Simon H-U, Haj-Yehia A, Levi-Schaffer F. Role of reactive oxygen species (ROS) in apoptosis induction. *Apoptosis*. 2000;5(5):415-418.
[45] Schrödinger suite 2014-3, *Schrödinger*, LLC New York, 2014.
[46] F. Ntie-Kang, An in silico evaluation of the ADMET profile of the StreptomeDB database, Springer Plus. 2 (2013).

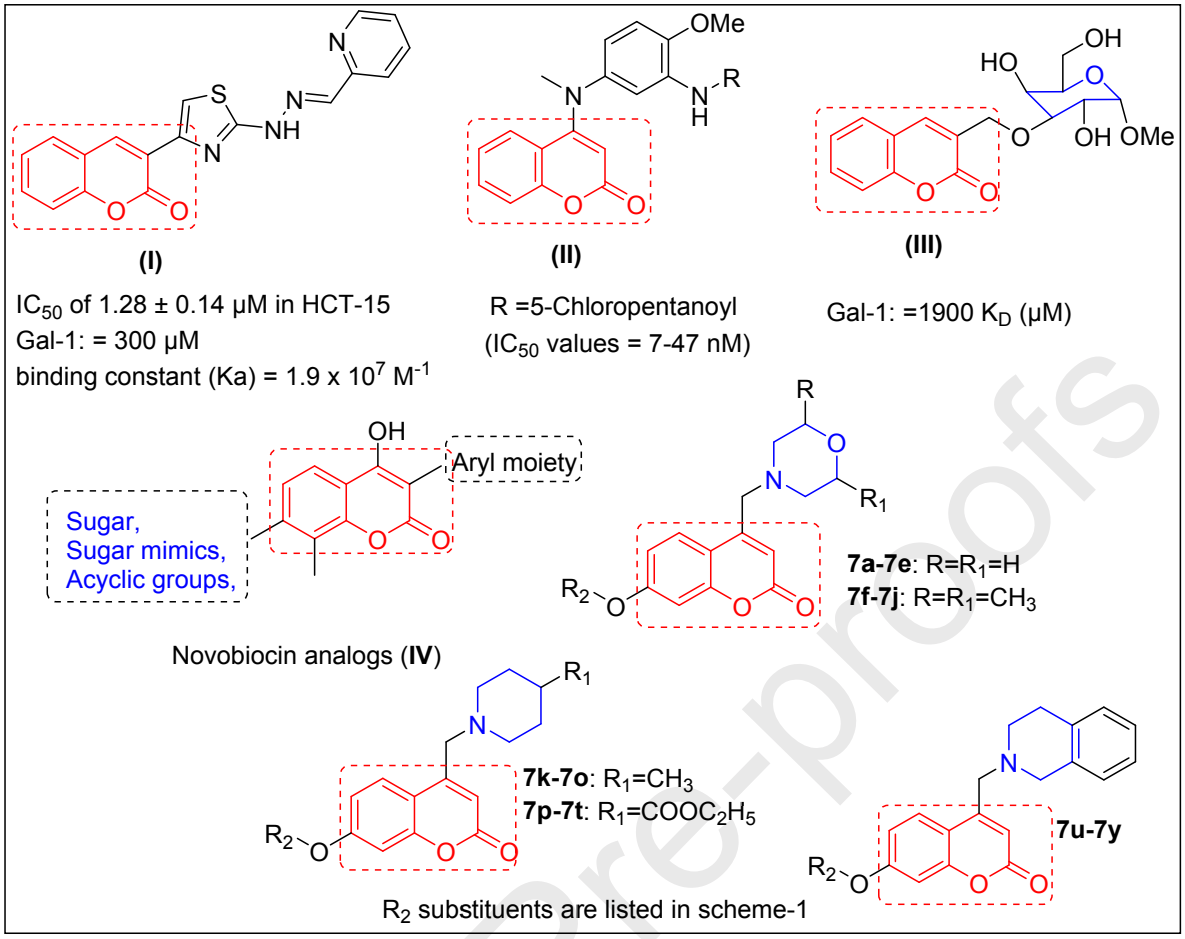

Figure 1. Representative examples of available coumarins as Gal-1 inhibitors and potent cytotoxic agents. Rationale for the designed target compounds **7a-7y**.

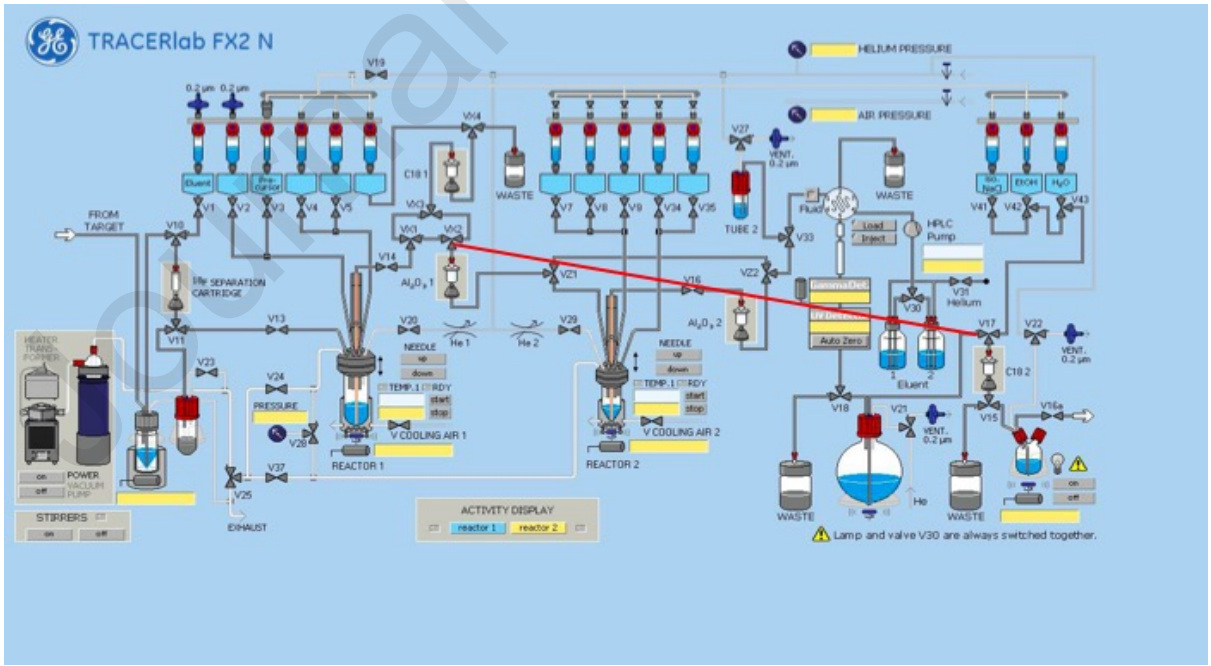

Figure 2. Scheme of the modified automated synthesizer GE Tracer-lab FX2N module. The left output of VX2 was connected to the V17.

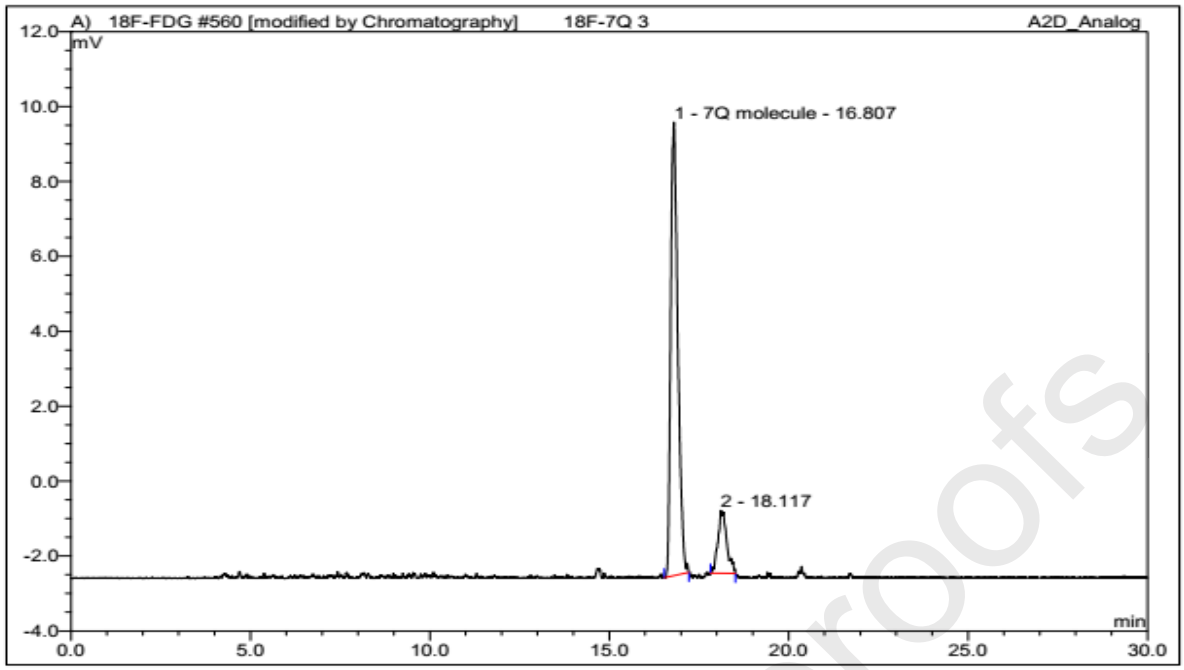

No.	Ret.Time min	Peak Name	Height mV	Area mV*min	Rel.Area %	Amount	Type
1	16.81	7Q molecule	12.105	2.769	85.31	0.812	BMB*
2	18.12	n.a.	1.674	0.477	14.69	n.a.	BMB*
Total:			13.779	3.246	100.00	0.812	

Figure 3A. Typical HPLC chromatogram of **[^{18}F]-7q** compound, detected by radio-detector.

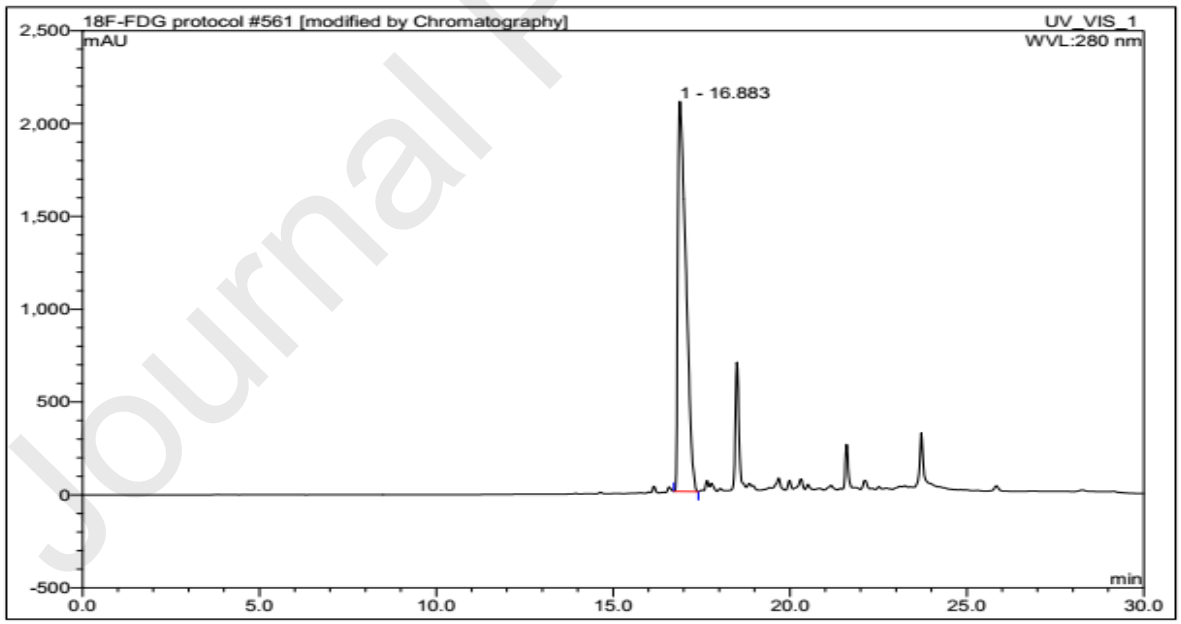

No.	Ret.Time min	Peak Name	Height mAU	Area mAU*min	Rel.Area %	Amount	Type
1	16.88	n.a.	2100.918	555.649	100.00	n.a.	BMB
Total:			2100.918	555.649	100.00	0.000	

Figure 3B. Typical HPLC chromatogram of the cold target compound, detected by UV-detector (280 nm).

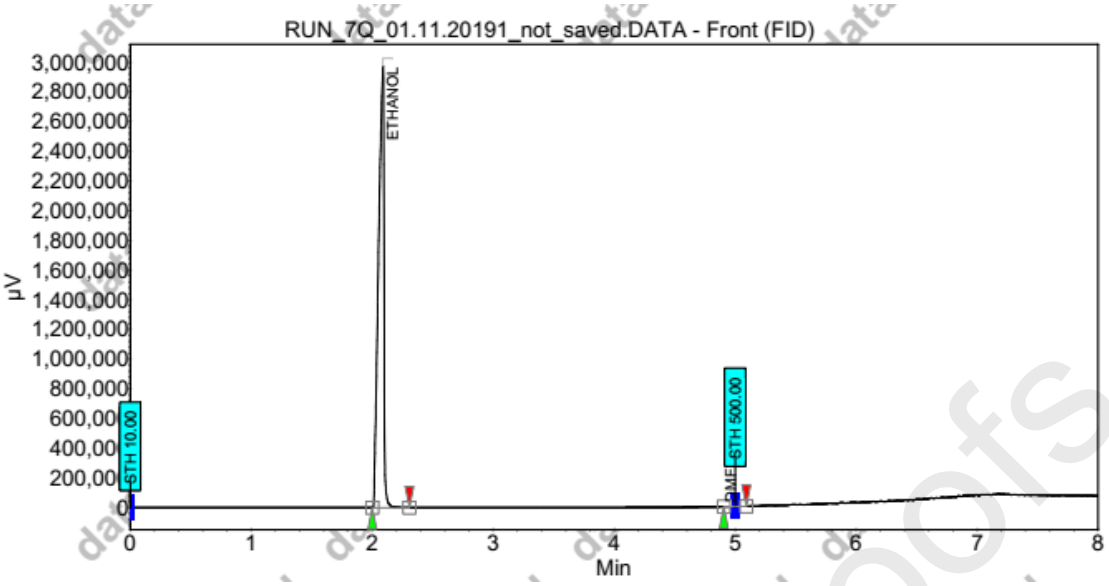

Peak results :

Index	Name	Time [Min]	Quantity [PPM]	Height [µV]	Area [µV.Min]	Area % [%]
1	ETHANOL	2.09	136175.13	2972269.3	152842.7	99.939
2	DMF	4.96	65.86	965.2	93.4	0.061
Total			136241.00	2973234.5	152936.1	100.000

Figure 4. The gas chromatography results of [^{18}F]-7q compound, which is showing the peaks of ethanol and DMF in ppm levels.

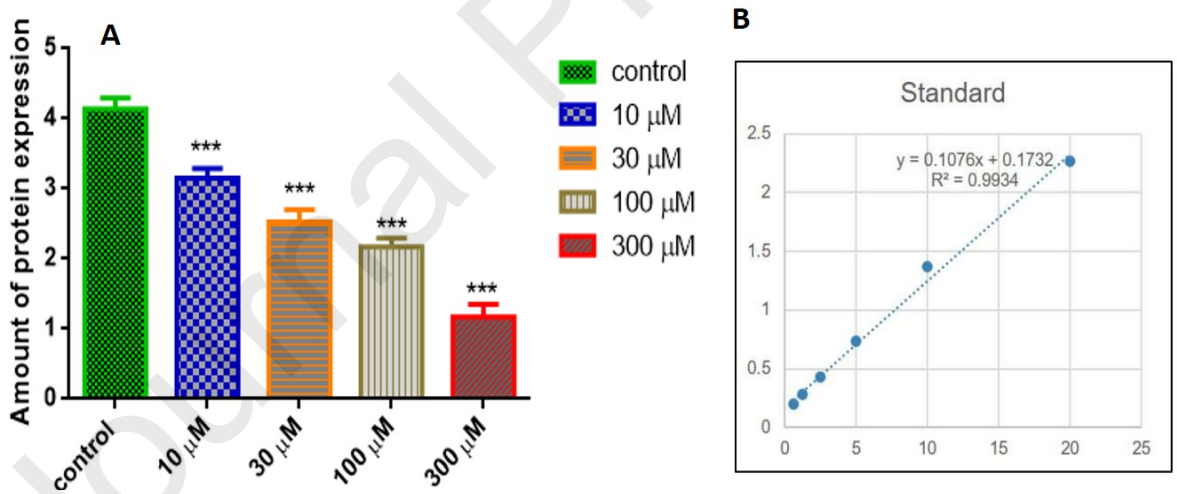

Figure 5: A) Gal-1 protein expression in PC-3 cells upon treatment with compound **7q** at 10, 30, 100 and 300 µM concentration. Untreated cells were considered for control evaluation. **B)** Graphical representation of Gal-1 standard protein.

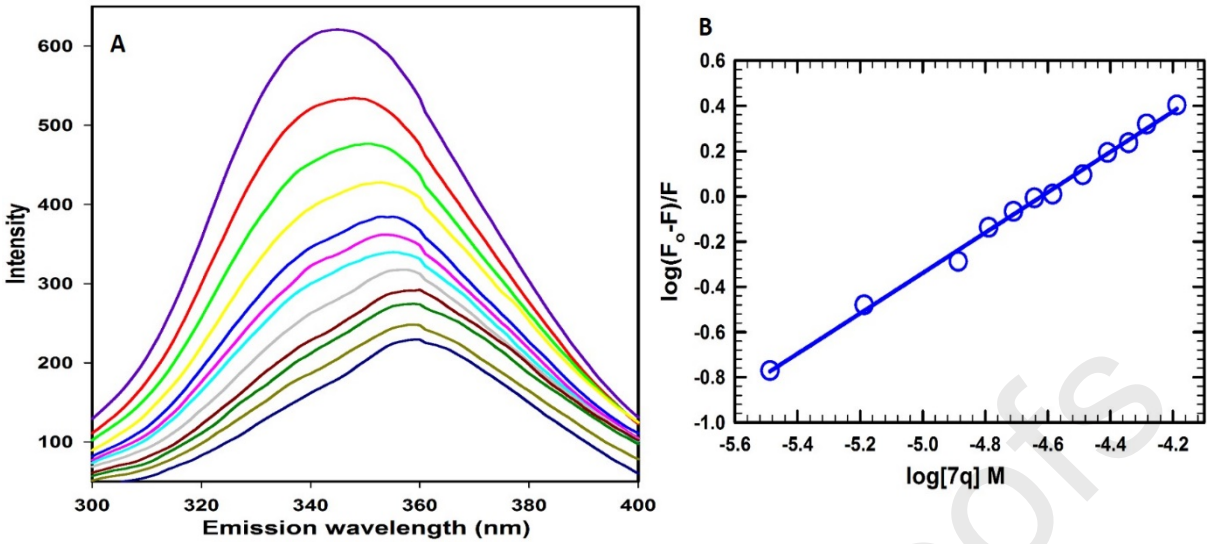

Figure 6: Fluorescence binding study of compound 7q with the Gal-1. **(A)** Fluorescence spectra of Gal-1 in the increasing concentrations of ligand from 0 to 65 µM (from top to bottom) at pH 7.5. The protein was excited at 280 nm and emission spectra was collected in the range of 300–400 nm. **(B)** Modified Stern–Volmer plot of Gal-1 by compound **7q** used for the calculation of binding affinity.

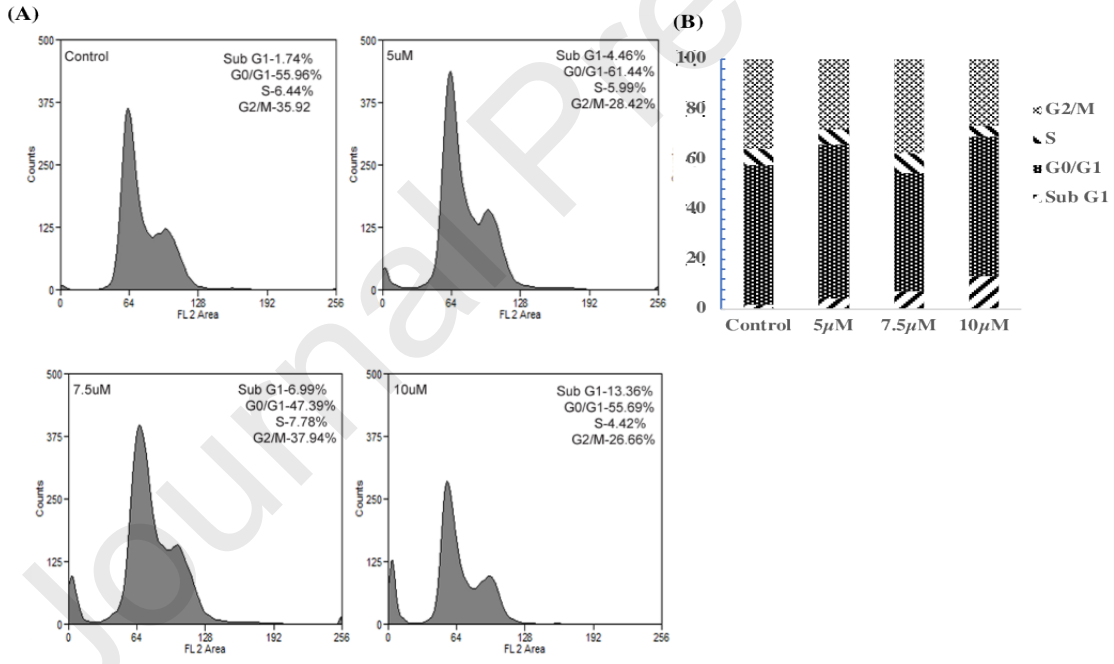

Figure 7: (A) Fluorescent based cell cycle analysis of PC-3 cells treated with conjugate **7q**. **(B)** Histograms depicting the phases of cell cycle post 48 h treatment at 5, 7.5 and 10µM concentrations.

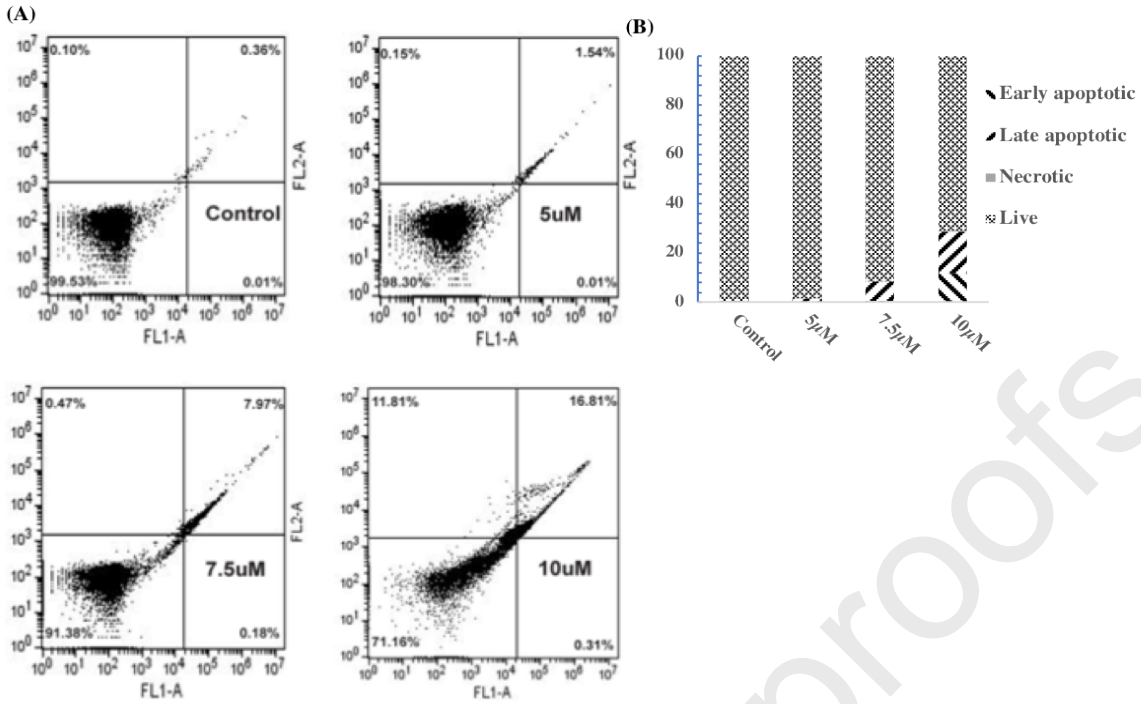

Figure 8: (A) Annexin-V Alexa fluor staining of PC-3 cells treated with conjugate **7q** for 48 h. Untreated cells were employed as controls. **(B)** Graphical representation of cells within the live and apoptotic populations.

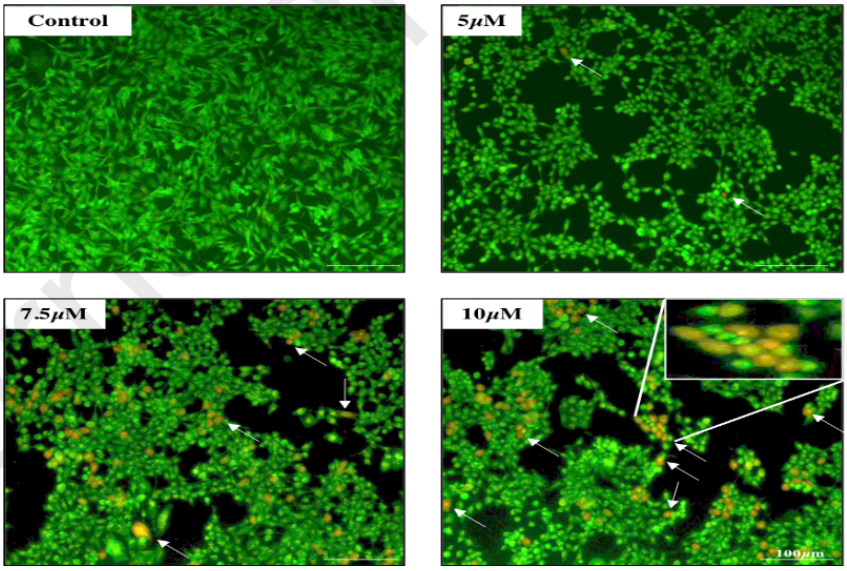

Figure 9: Fluorescent microscopic photos showing apoptotic effect of conjugate **7q** on PC-3 cells stained with Acridine Orange/Ethidium Bromide after 48 h of treatment. Untreated cells were utilized as controls. Cells were captured at 10X magnification. Scale bar indicates 100µm.

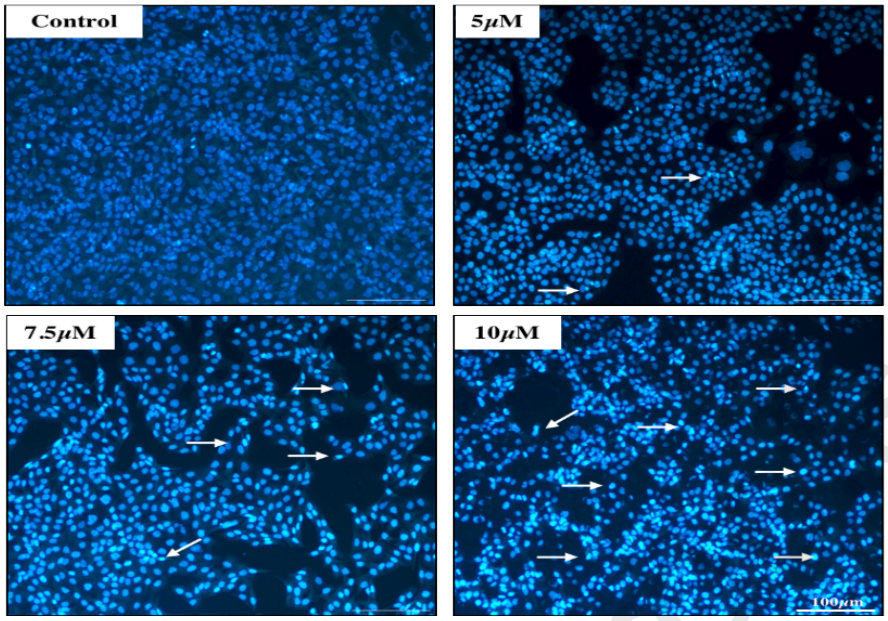

Figure 10: Effect of conjugate **7q** on nuclear morphology by Hoechst 33342 staining. Cells were treated for 48 h before imaging at 10X magnification. Scale bar indicates 100µm.

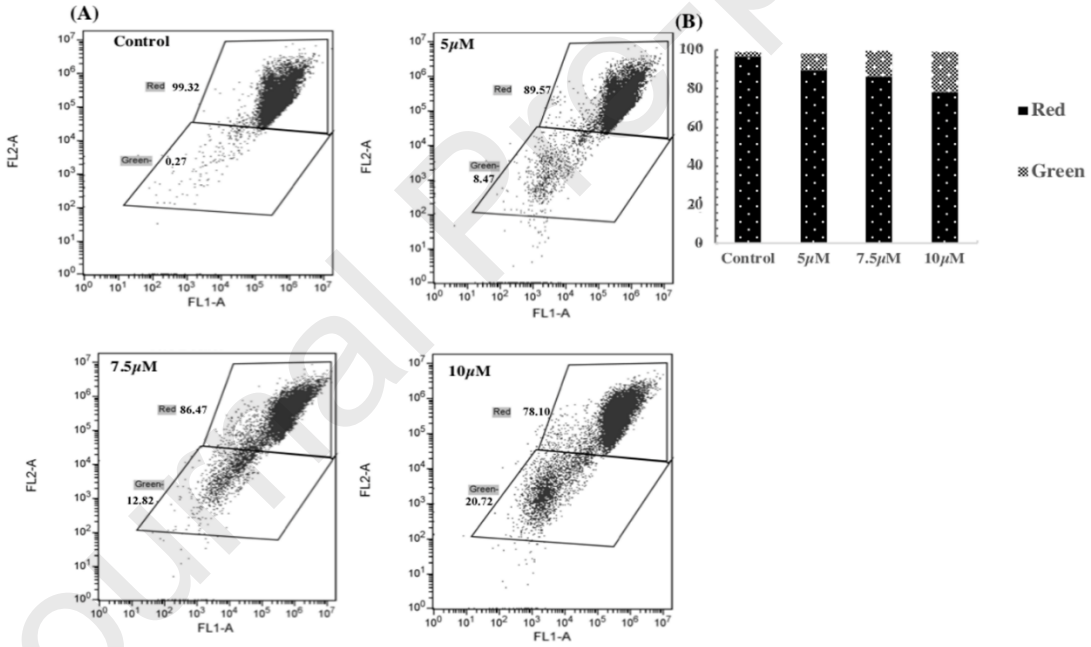

Figure 11: (A) Measurement of the mitochondrial membrane potential by flow cytometry using JC-1 dye in PC-3 cells post 48-h treatment with conjugate **7q**. **(B)** Graphical representation of the membrane potential among the untreated and treated cells. Untreated cells were used as controls.

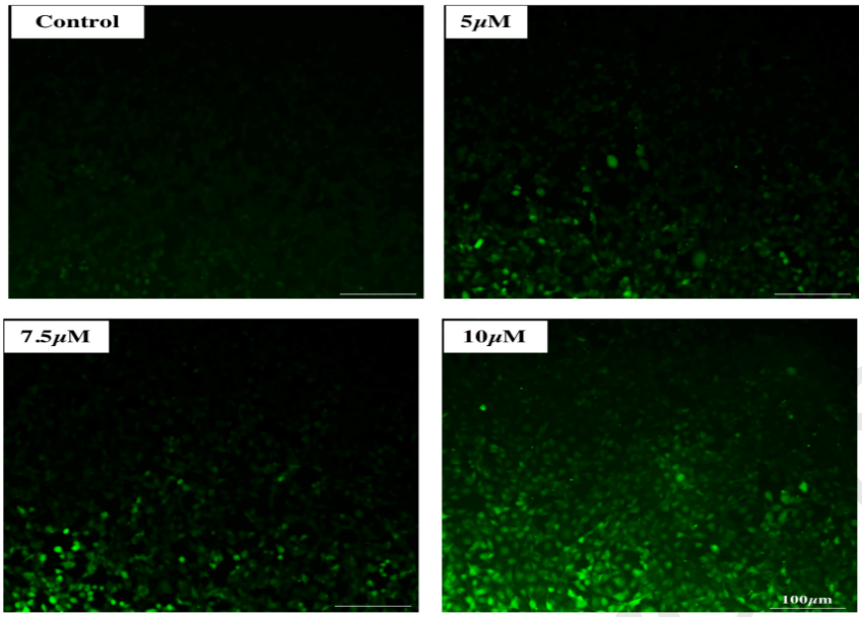

Figure 12: Estimation of reactive oxygen species (ROS) with DCFDA (2',7' – dichlorofluorescin diacetate) in conjugate **7q** treated PC-3 cells. Cells were imaged at 10X magnification post 48-h treatment. Scale bar indicates 100µm.

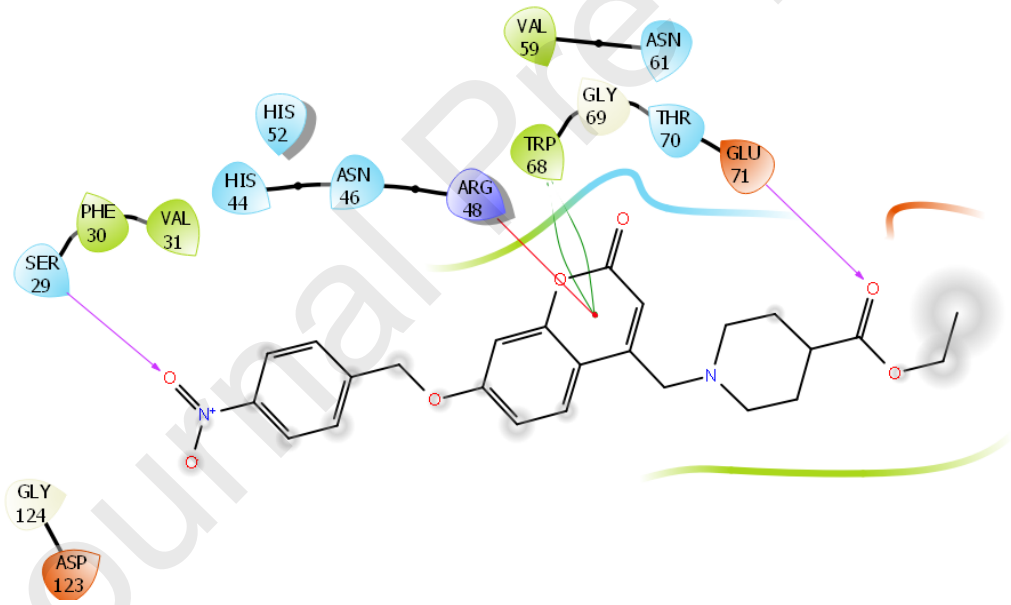

Figure 13A: 2D ligand interaction diagram of compound **7q** with the carbohydrate binding domain (CRD) of Gal-1 protein (PDB ID: 4Y24)

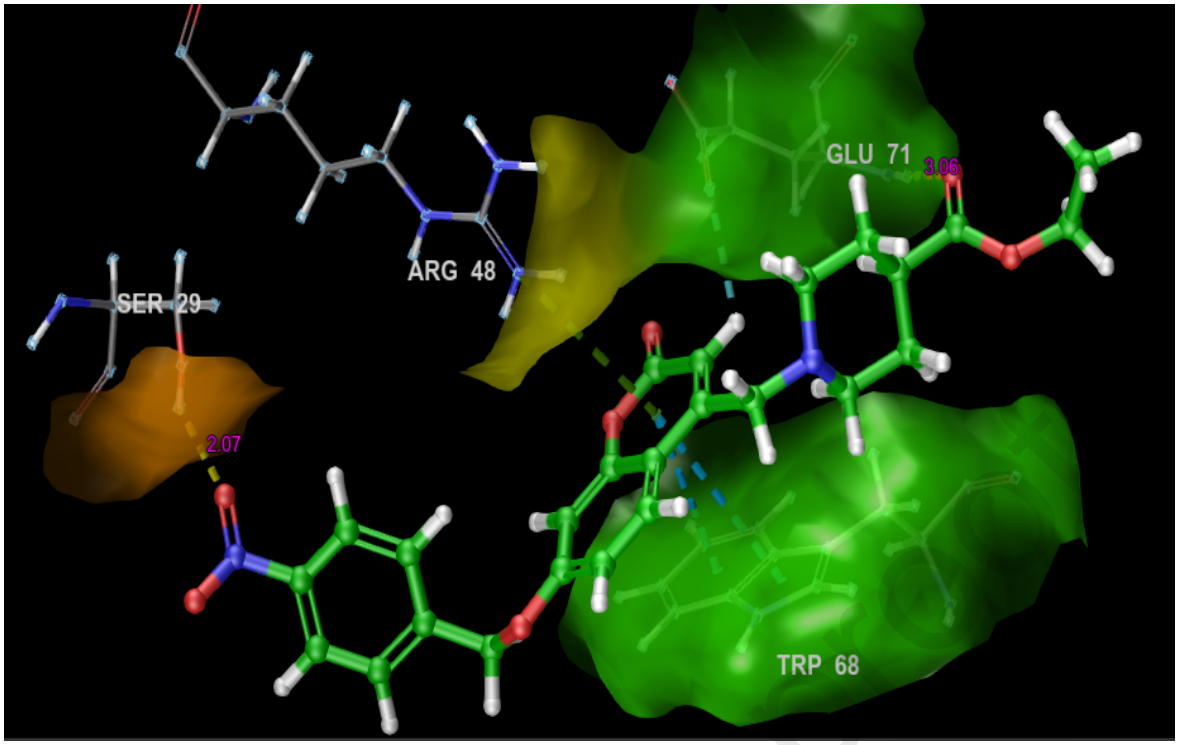

Figure 13B: 3D ligand interaction diagram of compound **7q** with the carbohydrate binding domain (CRD) of Gal-1 protein (PDB ID: 4Y24)

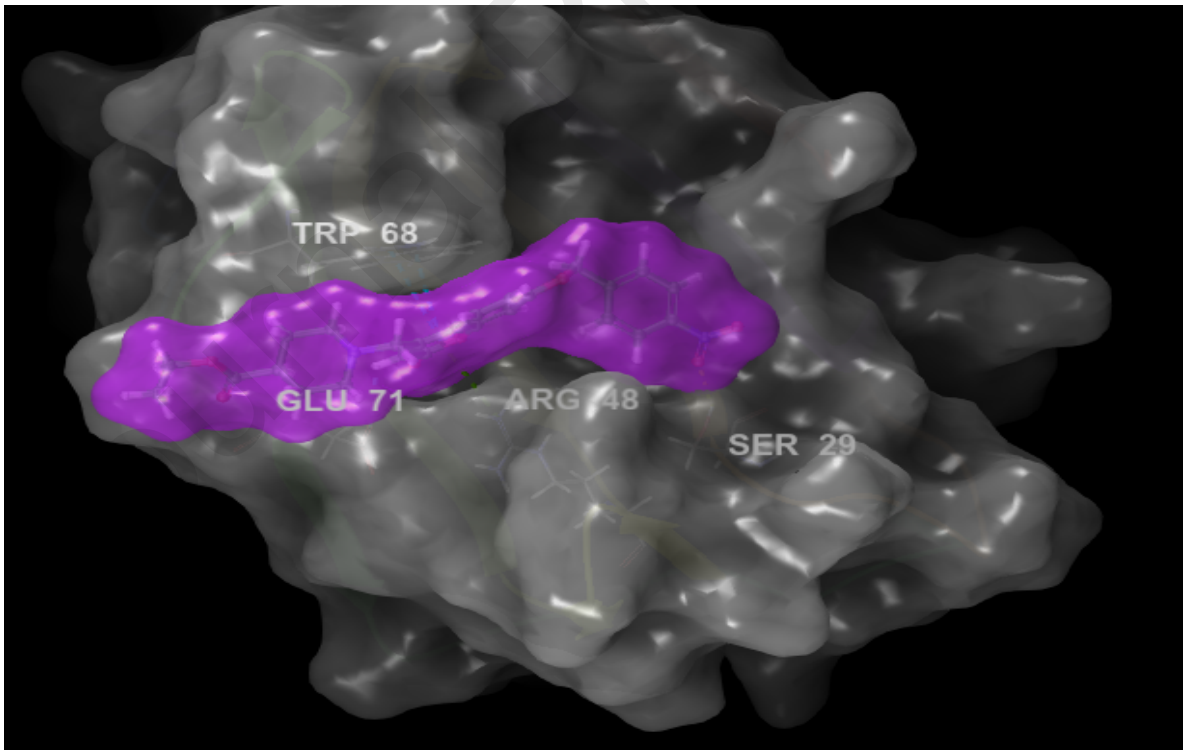

Figure 13C: Surface energy diagram of compound **7q** with the carbohydrate binding domain (CRD) of Gal-1 protein (PDB ID: 4Y24)

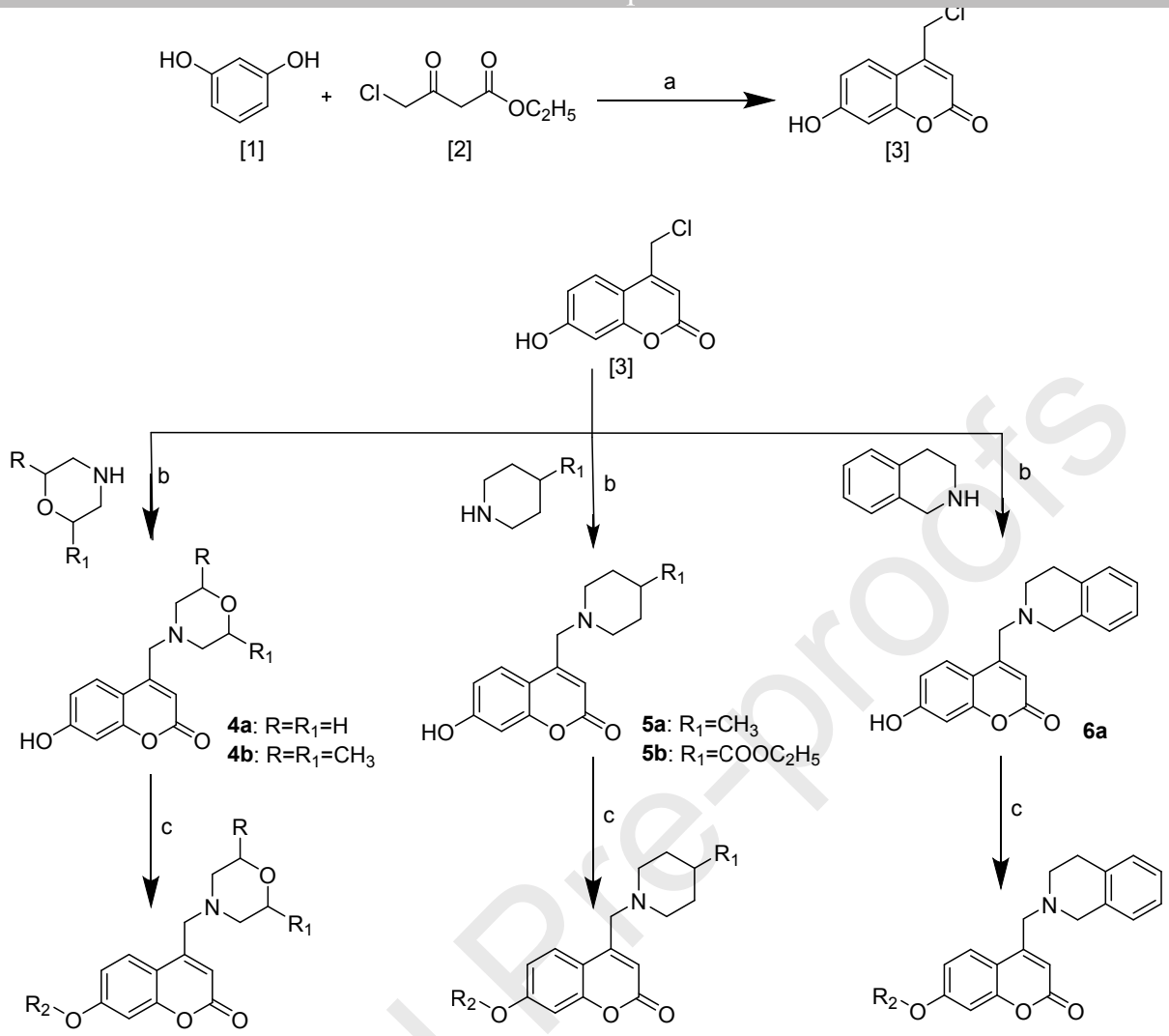

Scheme 1: Reagents and Conditions: a) conc H_2SO_4, 0-10 °C, 3h, 91-92% b) K_2CO_3, Acetone, 3-4 h, 82-88%. c) R_2X, K_2CO_3, Acetone, 3-4 h, 80-86%.

7a R_2 = 4-NO_2-C_6H_4-CH_2
7b R_2 = N≡C-CH_2
7c R_2 = CH≡C-CH_2
7d R_2 = 4-Br- C_6H_4-CH_2
7e R_2 = CH_2=CH-CH_2
7f R_2 = 4-NO_2-C_6H_4-CH_2
7g R_2 = N≡C-CH_2
7h R_2 = CH≡C-CH_2
7i R_2 = 4-CN-C_6H_4-CH_2
7j R_2 = CH_2=CH-CH_2

7k R_2 = 4-NO_2-C_6H_4-CH_2
7l R_2 = N≡C-CH_2
7m R_2 = 4-CN-C_6H_4-CH_2
7n R_2 = CH_2=CH-CH_2
7o R_2 = 4-Br- C_6H_4-CH_2
7p R_2 = C_6H_5-CH_2
7q R_2 = 4-NO_2- C_6H_4-CH_2
7r R_2 = 4-Br- C_6H_4-CH_2
7s R_2 = 4-OCH_3-C_6H_4-CH_2
7t R_2 = 4-CN-C_6H_4-CH_2

7u R_2 = 4-NO_2-C_6H_4-CH_2
7v R_2 = 4-Br- C_6H_4-CH_2
7w R_2 = 4-CN-C_6H_4-CH_2
7x R_2 = N≡C-CH_2
7y R_2 = CH_2=CH-CH_2

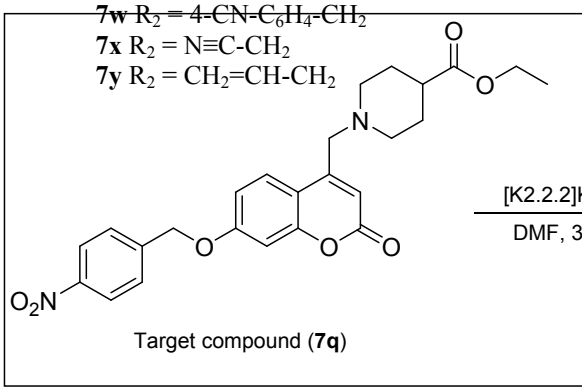

Target compound (**7q**)

Scheme 2. ^{18}F-radiolabeled target molecule synthesis *via* aromatic nucleophilic radio-fluorination of the compound 7q.

Table 1. IC_{50} (μM) values[a] of **7a-y** determined by SRB cell proliferation assay.

Compound	MCF7[b]	SKOV3[c]	PC-3[d]	DU145[e]	HEK293T[f]
7a	10.42 ± 0.14	11.09±0.09	17.05±0.07	15.83±0.13	-
7b	16.84±0.08	>30	22.3±0.07	18.035±0.3	-
7c	29.98±-0.13	>30	>30	17.91±0.14	-
7d	18.13±0.15	16.64±0.06	19.890±0.08	12.73±0.26	-
7e	26.89±0.15	13.34±0.11	19.17±0.04	15.82±0.23	-
7f	16.05±0.03	15.93±0.15	14.99±0.02	28.379±0.2	-
7g	>30	18.92±0.13	12.86±0.09	>30	-
7h	28.77±0.01	21.01±0.11	>30	29.98±0.2	-
7i	18.41±0.04	17.9±0.12	12.03±0.03	23.527±0.1	-
7j	>30	13.05±0.04	>30	17.16±0.2	-
7k	27.1±0.09	18.65±0.08	>30	16.52±0.3	-
7l	13.01±0.05	16.98±0.04	>30	16.495±0.1	-
7m	>30	>30	19.54±0.1	15.57±0.09	-
7n	>30	25.75±0.03	14.37±0.07	15.61±0.2	-
7o	>30	17±0.04	10.32±0.06	24.24±0.27	-
7p	>30	18.5±0.02	14.48±0.05	>30	-
7q	>30	14.63±0.05	7.45±0.03	8.95±0.17	>100
7r	>30	13.89±0.13	27.21±0.1	22.06±0.2	-
7s	26.36±0.07	12.33±0.06	11.82±0.13	11.38±0.06	-
7t	>30	12.18±0.03	16.01±0.07	28.14±0.1	-
7u	>30	>30	24.18±0.08	>30	-
7v	>30	14.33±0.19	28.955±0.11	>30	
7w	>30	>30	>30	>30	-
7x	>30	14.23±0.04	17.073±0.2	10.54±0.06	-
7y	13.74±0.03	24.64±0.07	>30	29.893±0.1	-
Doxorubicin	1.22±0.02	2.95±0.1	2.54±0.03	0.53±0.21	

[a] 50% Inhibitory concentration after 72 h of drug treatment. [b] Human breast cancer. [c] Human ovarian cancer. [d] Human prostate cancer. [e] Human prostate cancer. [f] Human embryonic kidney (Normal cells).

Table 2. Amount of galectin-1 protein expression in control and compound **7q** (10, 30, 100 and 300 μM) treated PC-3 cells.

Concentration (μM)	**Absorbance at 450 nm**	**Galectin-1 concentration(μg/mL)**
Control	0.6074575	4.03±0.4
7q (10)	0.501731	3.10±0.5
7q (30)	0.4404215	2.40±0.5
7q (100)	0.397062	2.08±0.32
7q (300)	0.2863535	1.05±0.52

Table 3: *The physicochemical properties (ADMET) of* **7q** compound *were calculated using qikprop program* are listed below.

S. No	**Properties or Descriptors**	**Recommended Values**	**Compound 7q**
1	Molecular weight	130.0 – 725.0	440.284
2	Dipole moment	1.0 – 12.5	25.339
3	Total SASA	300.0 – 1000.0	749.571
4	Molecular Volume	500.0 – 2000.0	1282.734
5	No. of rotatable bonds	0 – 15	8
6	Donor HB	0.0 – 6.0	0
7	Acceptor HB	2.0 – 20.0	7.5
8	QP Polarizability	13.0 – 70.0	44.038
9	QP logP o/w	2.0 – 6.5	2.771
10	QP log BB	-3.0 – 1.2	-2.791
11	QP log HERG	Concern below -5	-7.383
12	Human Oral Absorption	1-3	3
13	Percent Human Oral Absorption	>80% is high	72.266
14	Rule of Five violations	<25% is low	0
15	No. of metabolites	Maximum of 4	2

Synthesis, ^{18}F-Radiolabeling and Apoptosis Inducing Studies of Novel 4, 7-Disubstituted Coumarins

Nerella Sridhar Goud [a, b], Venkata Krishna Kanth [c], Jakkula Pranay [e], Ravi Alvala [d], Insaf A. Qureshi [e], Pardeep Kumar [b], Rose Dawn Bharath [b], Chandana Nagaraj [b], Suresh Yerramasetti [c], Manika Pal-Bhadra [c], Mallika Alvala [a]*

[a] Department of Medicinal Chemistry, National Institute of Pharmaceutical Education and Research (NIPER), Hyderabad 500 037, India.

[b] Department of Neuroimaging and Interventional Radiology (NI & IR), National Institute of Mental Health and Neuro Sciences (NIMHANS), Bangalore 560 029, India.
[c] Department of Applied Biology, CSIR-Indian Institute of Chemical Technology, Hyderabad 500 007, India.
[d] G. Pulla Reddy College of Pharmacy, Hyderabad 500 028, India.
[e] Department of Biotechnology & Bioinformatics, School of Life Sciences, University of Hyderabad, Hyderabad 500 046, India.

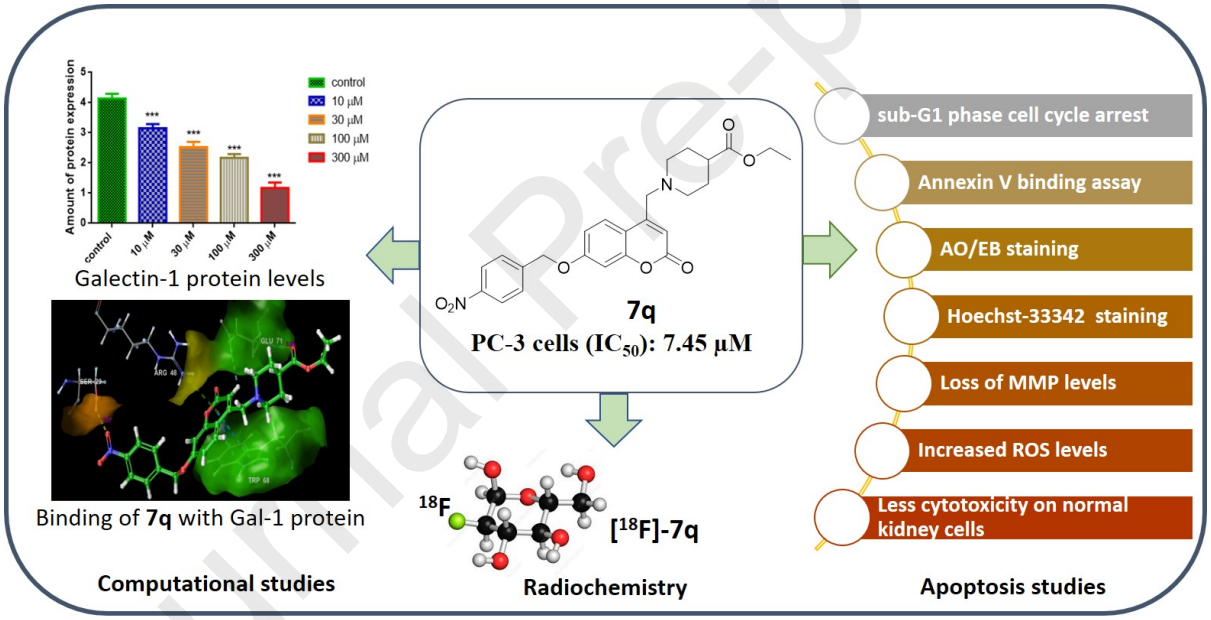

Research Highlights:

- The **7q** is a novel anticancer agent with an IC_{50} of 7.45±0.03 μM mediated by Gal-1 in PC-3 cells.
- Identified novel **7q** molecule which induces apoptosis *via* Gal-1 reduction in PC-3 cells.
- The **[^{18}F]-7q** radiotracer is an ideal PET imaging agent due to its optimal half-life of 110 min.
- The radiochemical identity and purity were confirmed as per cGMP guidelines for clinical use.

Declaration of interests

☒ The authors declare that they have no known competing financial interests or personal relationships that could have appeared to influence the work reported in this paper.

☐The authors declare the following financial interests/personal relationships which may be considered as potential competing interests:

Nil